AFRL-IF-RS-TR-2005-304
Final Technical Report
August 2005

MOLECULAR ENGINEERING OF SURFACES FOR SENSING AND DETECTION

University of Washington

Sponsored by
Defense Advanced Research Projects Agency
DARPA Order No. K900

AIR FORCE RESEARCH LABORATORY
INFORMATION DIRECTORATE
ROME RESEARCH SITE
ROME, NEW YORK

STINFO FINAL REPORT

This report has been reviewed by the Air Force Research Laboratory, Information Directorate, Public Affairs Office (IFOIPA) and is releasable to the National Technical Information Service (NTIS). At NTIS it will be releasable to the general public, including foreign nations.

AFRL-IF-RS-TR-2005-304 has been reviewed and is approved for publication

APPROVED: /s/

THOMAS E. RENZ
Project Engineer

FOR THE DIRECTOR: /s/

JAMES A. COLLINS, Acting Chief
Advanced Computing Division
Information Directorate

REPORT DOCUMENTATION PAGE

Form Approved
OMB No. 074-0188

1. AGENCY USE ONLY (Leave blank)	2. REPORT DATE	3. REPORT TYPE AND DATES COVERED
	AUGUST 2005	Final Jun 01 – Jan 05

4. TITLE AND SUBTITLE
MOLECULAR ENGINEERING OF SURFACES FOR SENSING AND DETECTION

5. FUNDING NUMBERS
C - F30602-01-2-0542
PE - 61101E
PR - E117
TA - 00
WU - 71

6. AUTHOR(S)
Shaoyi Jiang

7. PERFORMING ORGANIZATION NAME(S) AND ADDRESS(ES)
University of Washington
Department of Chemical Engineering
Seattle Washington 98195

8. PERFORMING ORGANIZATION REPORT NUMBER
N/A

9. SPONSORING / MONITORING AGENCY NAME(S) AND ADDRESS(ES)
Defense Advanced Research Projects Agency
3701 North Fairfax Drive
Arlington Virginia 22203-1714

AFRL/IFTC
525 Brooks Road
Rome New York 13441-4505

10. SPONSORING / MONITORING AGENCY REPORT NUMBER
AFRL-IF-RS-TR-2005-304

11. SUPPLEMENTARY NOTES
AFRL Project Engineer: Thomas E. Renz/IFTC/(315) 330-3423/ Thomas.Renz@rl.af.mil

12a. DISTRIBUTION / AVAILABILITY STATEMENT
APPROVED FOR PUBLIC RELEASE; DISTRIBUTION UNLIMITED.

12b. DISTRIBUTION CODE

13. ABSTRACT ***(Maximum 200 Words)***

There are three challenges in the development of surfaces for sensing and detection - sensitivity (i.e., low detection limit), specificity (i.e., false positives and negatives), and robustness (simultaneous detection of multiple analytes). These three issues are addressed in this work with the main focuses on control of protein orientation and creation of protein arrays.

The ability to control, probe, and predict protein orientation will facilitate the development of biosensors with high sensitivity and specificity. In this work, a charge-driven protein orientation principle was proposed. Molecular simulations were first performed to predict protein orientation on a surface under a wide range of conditions. Simulation results showed that there is indeed a distinct difference in protein orientation on different charged surfaces. Surface Plasmon Resonance (SPR) and Time-of-Flight Secondary Ion Mass Spectrometry (ToF-SIMS) experiments were then performed to confirm simulation results.

Protein arrays are an attractive platform for many applications in sensing and detection, yet due to challenges with fabrication, storage, and protein stability they have not realized their full potential. In this work, a novel single stranded DNA probe surface is introduced, which when used in conjunction with a simple DNA-antibody conjugate, produces a biosensor surface with superior sensitivity, protein resistance and chip stability.

14. SUBJECT TERMS
Self Assembled Monolayers, Bioagent Detection, Biosensors, DNA Probe, Protein Orientation

15. NUMBER OF PAGES
95

16. PRICE CODE

17. SECURITY CLASSIFICATION OF REPORT	18. SECURITY CLASSIFICATION OF THIS PAGE	19. SECURITY CLASSIFICATION OF ABSTRACT	20. LIMITATION OF ABSTRACT
UNCLASSIFIED	UNCLASSIFIED	UNCLASSIFIED	UL

Table of Contents

List of Figures

List of Tables

Summary

There are three challenges in the development of surfaces for sensing and detection - sensitivity (i.e., low detection limit), specificity (i.e., false positives and negatives), and robustness (simultaneous detection of multiple analytes). When a protein is immobilized on a surface, the first challenge is to control its orientation and conformation so as to preserve its bioactivity while the second challenge is to control its nonspecific adsorption, particularly in complex media. Furthermore, it is desirable to create multiple functional spots in one flow channel so as to perform the simultaneous detection of multiple analytes. However, all current surface chemistries are not selective. This work addresses all three issues with the main focus on control of protein orientation and creation of protein arrays.

The ability to control, probe, and predict protein orientation will facilitate the development of biosensors with high sensitivity and specificity. In this work, a charge-driven protein orientation principle was proposed. Monte Carlo (MC) simulations were first performed to predict protein orientation on a surface under a wide range of conditions. Three-level models were used, a 12-bead model, reside-model and all-atom model. Simulation results show that there is indeed a distinct difference in protein orientation on different charged surfaces. Surface Plasmon Resonance (SPR) and Time-of-Flight Secondary Ion Mass Spectrometry (ToF-SIMS) experiments were then performed to confirm simulation results. Furthermore, combined MC and Molecular Dynamics (MD) simulations were performed to study protein conformation. The charge-driven protein orientation principle has been proven to be very useful for control of a wide range of proteins for their orientations (typically smaller and harder proteins). Ligand-receptor interactions were also studied using a hybrid simulation technique.

Protein arrays are an attractive platform for many applications in sensing and detection, yet due to challenges with fabrication, storage, and protein stability they have not realized their full potential. This work introduced a novel ssDNA probe surface, which when used in conjunction with a simple DNA-antibody conjugate, produces a biosensor surface with superior sensitivity, protein resistance and chip stability. The ssDNA probe surface is a mixed Self Assembled Monolayer (SAM) of ssDNA and oligo ethylene glycol (OEG) terminated thiols or the sensor platform is based on biotinylated single-stranded DNA immobilized via a streptavidin bridge to a mixed SAM of biotinylated alkanethiol and OEG. This technology will allow one to store a chip as a DNA chip and to use the chip as a protein chip.

Through DARPA support, two major capacities were developed. One is a biosensor

technology capable of the quantitative and simultaneous detection of multiple analytes in complex media with high sensitivity and specificity. Currently, this technology has been applied for a range of applications, particularly for food safety and security monitoring, and biomedical diagnostics. Another is a computational capability to study and design biological interfaces using different models and simulation techniques.

Introduction

Proper orientation of antibodies on surfaces is critical to the performance of biosensors, especially for rapid and sensitive bioassay methods, such as SPR biosensors and quartz crystal microbalances. Better control of antibody orientation on surfaces will enhance both the total response and the response kinetics, thus improving the performance of monolayer-based biosensors. From a broader perspective, the orientation of adsorbed proteins on surfaces is also critical to many bio-related applications, such as biomaterials. Properly orientated cell-adhesive proteins on surfaces are expected to dramatically boost the performance of biomaterials for wound healing and biocompatibility. Thus, it is desirable to control the orientation of proteins on surfaces. Protein behavior on surfaces has been studied for decades. However, controlling protein orientation is still very challenging. This is due to a lack of not only approaches for systematic control of microenvironments, but also general methods to characterize protein orientation. Some previous studies of protein orientation by physical adsorption showed that protein orientation might be affected by surface charge. Buijs and co-workers [1] found that the antigen/antibody ratio was very low on negatively charged surfaces, likely due to undesirable orientation. Edmiston and co-workers [2] showed some preferred orientations of cytochrome C on Langmuir-Blodgett films. It was also reported that IgY had better orientation on negatively charged polymer surfaces. These studies indicate that charge may play an important role in protein orientation. In parallel, other studies showed that protein could be oriented via hydrophobic patches on protein [3] and by the Langmuir-Blodgett method [4]. Due to a lack of systematically controllable systems at the molecular level, it is difficult to conclude how various forces (e.g., electrostatic and hydrophobic forces) affect protein orientation. For example, Buijs and coworkers [1] studied antibodies on negatively charged silica and hydrophobic polymeric surfaces. These surfaces were controlled and characterized at the macroscopic level. Since proteins have distinct shapes and surface functionalities, molecular details of the surface are of great importance to protein adsorption. Protein behavior on surfaces is determined by molecular-scale interactions of protein molecules with the surface. In the work by Edmiston and co-workers [2], only those proteins with optically active porphyrin could be studied. For the hydrophobic-patch method [3], the difference in electrochemical current might be caused by the difference in enzyme denaturation on bare gold versus on hydrophobic SAM surfaces, and the difference in electron transfer in these two different systems. For the Langmuir-Blodgett method [4], adsorbed antibody layers were more easily denatured due to the exposure of F_{ab} fragments to air at the air-liquid interface. Denatured antibodies would cause nonspecific adsorption, thus lowering the specificity and sensitivity of biosensors. Thus, one

of the main objectives of this work is to predict, control and probe protein orientation and conformation on well-controlled surfaces.

There is an urgent demand for development of multi-channel biosensors, which enable accurate and simultaneous detection, identification, and monitoring of multiple proteins in a given biological sample for medical diagnostics in additional to food and drug screening, environmental protection, and homeland security. Surface functionalization of biosensor chips is critical to the performance of biosensors. However, there are many critical issues faced in biosensor technology today, such as simultaneous detection of multiple analytes, chip storage, detection limit, and reliability. Biosensors often require immobilization of antibodies on a solid support. Micro-spotting or contact printing is commonly used to functionalize different antibodies on multiple spots. These methods deposit the desired antibody directly onto the surface of the chip. Storage of these chips is a very serious issue as antibodies easily become denatured and unstable on the chips. Many of current micro-spotting technologies have direct contact between pin and surface. It is difficult to control antibody orientation, conformation, and bioactivity when they are spotted on the surface via chemical link or physical adsorption. These protein chips are produced for a single, specific use because of prescribed types of antibodies on the chips. For some field applications, chip regeneration may be desirable. However, chip regeneration is not practical for conventional chips since it is hard to strip antigen completely from an antibody and to remove covalently bound antibody from a surface. Thus, one of the main objectives of this work was to develop a robust protein immobilization technique capable of creating multiple functional spots on one flow channel.

Methods, Assumptions, and Procedures

For molecular simulation studies of protein orientation and conformation, there are three-level protein models – (a) 12-bead model, (b) residue-model, and (c) all-atom model while there are two simulation methods (a) MC and MD simulations. While MC simulations are used to study protein orientation on a surface, MD simulations are used to study protein conformation. The 12-bead model is very useful to qualitatively map out how various factors affect protein orientation. The residue model is needed to quantitatively study the orientation of a specific protein (e.g., IgG1 or IgG2a). For the study of protein conformation, the all-atom model is needed.

For experimental studies of protein orientation, two methods were used – (a) SPR and ToF-SIMS. While SPR can provide indirect information about protein orientation via probing antigen response to the immobilized antibody, ToF-SIMS can provide direct evidence of protein orientation via probing the molecular composition of the immobilized

antibody within the topmost 1-1.5nm.

To create protein arrays, the ssDNA probe surface is a mixed SAM of ssDNA and OEG terminated thiols or the sensor platform is based on biotinylated single-stranded DNA immobilized via a streptavidin bridge to a mixed SAM of biotinylated alkanethiol and OEG.

MC Simulations of Protein Orientation Based on a Twelve-Bead Model: IgG is one kind of protein that conforms to a common subunit structure. It is composed of four chains (two heavy chains and two light chains) that are connected by disulfide bonds and noncovalent forces. The four chains are grouped together in different fragments - two identical F_{ab} fragments and one F_c fragment, forming a Y-shape conformation. Each fragment has four domains. Thus, we could model an antibody as a 12-bead structure, for which the angle between two F_{ab} fragments is fixed to 90^o. As a first approximation, we consider the antibody as a rigid structure. Each bead is treated as a sphere of 3.0 nm diameter with the net charge placed at its center. The proposed model gives a reasonable approximation of the aspect ratio of an antibody molecule. In this work, each C_H3 (constant region 3 of heavy chain of an antibody) domain carries –2e charge, whereas each V_L (variable region of the light chain of an antibody) domain carries +2e charge. The adsorption substrate consists of 1440 surface atoms within an area of $17.98nm \times 17.30nm$. Among these surface atoms, 72 are randomly selected to carry a charge of +e (or –e) to represent positively (or negatively) charged surfaces. Other surface atoms are neutral. This corresponds to a surface charge density of +/- $0.037C/m^2$. The Lennard-Jones (LJ) radius and well-depth parameters of the surface atoms are the same as those used by Ravichandran et al. [5], 1.85Å and 0.152kcal/mol.

MC Simulations of Protein Orientation Based on a Residue Model: In our proposed united-residue model, each amino acid was reduced to a single sphere centered at the α -carbon position. Thus, the basic structure characters of two antibodies could still be kept. The protein structure was assumed rigid. Self-assembled monolayers (SAMs) are ideal platforms for protein adsorption studies and biosensor applications. Thus, we selected SAM as the model surface for the development of protein-surface interaction potential, which consisted of both Van Der Waals (VDW) and electrostatic interactions.

MC simulations were carried out in a box of $30nm \times 30nm \times 30nm$. The residue-based protein-surface interaction potentials were used. The temperature of the simulated system was 298K. Only one antibody molecule was considered in simulations. Since the net charges of the two antibodies are both zero, the pH value of the simulated system corresponds to the isoelectric point of each antibody. Initially, the antibody was put 10nm above the surface with a random orientation. During simulations, the protein was translated and rotated around its center of mass. The displacement of each move was adjusted to ensure

an acceptance ratio of 0.5. At each condition, 10-30 simulations were performed to explore multiple orientations. Results reported in this study were usually averaged over two million configurations.

MD Simulations of Protein Conformation Based on an All-Atom Model: Cyt-c consists of 104 residues and 1 heme ring. The high-resolution crystal structure of horse heart Cyt-c (PDB code: 1HRC), refined to 1.9Å by Bushnell et al. [6], served as the starting point of the simulation. Hydrogen atoms were added by the Chemistry at HARvard and Molecular Mechanics (CHARMM) package found at http://yuri.harvard.edu/. For the all-atom structure of Cyt-c, there are total 1744 atoms. The protein was simulated at pH 7.0. The N-terminus of Cyt-c was acetylated. The arginine (ARG) and lysine (LYS) residues were taken to be protonated whereas glutamic acid (GLU) and aspartic acid (ASP) residues along with the C-terminus were taken to be deprotonated. The histidine (HIS) adopts the neutral protonation state (HSD) in this work. For the Fe-S bond, bond length used is 2.32Å while force constant 65.0kcal·mol^{-1}·Å^{-2}. The protein has a net charge of +6e. Only one protein molecule was considered in simulations. The potential parameters for Cyt-c are from the CHARMM force field for proteins. For the surface, the $\sqrt{3}\times\sqrt{3}$ structure of HS(CH_2)$_9$COOH SAMs on Au(111) was adopted, which consist of 168 thiol chains and 1512 gold atoms,. For thiol chains in the studied systems, 8, 42, or 84 chains are deprotonated, representing a 5%, 25%, or 50% dissociation degree of negatively charged SAMs, respectively. Chen et al. [7] chose SAMs terminating in SO_3^- group as a charged surface in their experiments, which should have a higher surface charge density than that of COOH SAMs. For simplicity, we used COO- SAMs with different dissociation degrees to represent various negatively charged surfaces. The surface has a dimension of 59.94Å×60.4Å. The potential parameters for SAMs are from the CHARMM force field for lipids.

For MC simulations, initially, the center of mass of the protein was put 5nm above the surface with a random orientation. During simulations the protein was kept rigid. It was translated and rotated around its center of mass. The displacement of each move was adjusted to ensure an acceptance ratio of 0.5. With the preliminarily optimized orientation of Cyt-c on SAM surfaces from MC simulations, water molecules were added to a simulated box of 59.94Å×60.4Å×61.0Å. The added water molecules were selected such that no water oxygen atom was closer than 2.8Å to the protein and surfaces. There are 4160 water molecules in the system, which are described by the TIP3P model. To keep the system neutral, 6 chlorines were added to the simulated box with 8, 42, and 84 sodium ions for carboxyl-SAM surfaces with a dissociation degree of 5%, 25%, and 50%, respectively. The ions are modeled by a potential proposed by Beglov and Roux [8]. Each simulation system has total 21622 atoms. The gold atoms and the sulfur atoms of SAMs were kept fixed during

simulations. Bonds containing hydrogen were kept rigid using the RATTLE method with a geometric tolerance of 10^{-6}. The short-range non-bonded interactions were calculated by a switched potential with a switching function starting at 10Å and reaching zero at a distance of 11Å. Electrostatic interactions were calculated by the shifted potential with a cutoff distance of 11Å. Two-dimensional periodic boundary conditions were used in the simulations. There is a hard wall on the top of the simulation box and a reflective boundary condition is applied. Each MD simulation was carried out over a period of 1ns with a time-step of 1fs.

SPR Study of Protein Orientation on Charged Surfaces: Gold-coated substrates were modified by pure or mixed SAMs with different terminal groups. SAMs were formed by soaking gold-coated substrates in 100% ethanol solution of thiol (total concentration ~1 mM) at room temperature or 65^{o}C after careful cleaning of the chips. The cleaning procedure included: washing gold-coated substrates by chloroform and 100% ethanol, cleaning under UV light, and washing by DI water and 100% ethanol. The substrates remained in the thiol solution overnight to form complete SAMs. After SAMs were formed, the chips were washed by ethanol, 1:10 (v/v) acetic acid ethanolic solution, and ethanol again.

Immulogical activity was determined as follows. SPR was first stabilized by 2mM PBS solution. Then, 13.2 μg/ml anti-Human Choriogonadotropih (hCG) was flowed into SPR for 20 minutes, followed by flushing with 2mM PBS solution for 5 minutes to remove irreversibly bound antibodies. Adsorbed anti-hCG was chemically immobilized by 0.05% glutaradehyde in 2mM PBS for 10 minutes. To block non-specific binding sites, 0.25mg/ml BSA was flowed for 20 minutes. Finally, 1 μg/ml hCG in 0.25mg/ml BSA PBS solution was flowed for 15 minutes, followed by flushing with 0.25mg/ml BSA solution for 10 minutes. A typical SPR response curve is shown in Figure 1 when 50μg/ml hCG was used. Nonspecific reaction was checked by replacing anti-hCG with anti-bacterial alkaline phosphatase for the experiment shown in Figure 1. No detectable hCG binding was found.

ToF-SIMS Study of Protein Orientation: ToF-SIMS analysis was conducted using a Model 7200 Physical Electronics reflectron time-of-flight secondary ion mass spectrometer (PHI, Eden Prairie, MN) with an 8 keV Cs^{+} primary ion source. Positive and negative ion spectra were acquired from 0 to 200 m/z and from 0 to 1000 m/z, respectively over an area of 100 μm x 100 μm with a primary ion dose of less than 10^{12} ions/cm^2 to ensure static ToF-SIMS conditions. The mass resolution (m/Δm) at the $C_4H_8N^{+}$ (m/z = 70) and C_2H^{-} (m/z = 25) peaks were typically above 4500. At least three replicates were performed for each sample, with at least three spectra recorded on each replicate. Only spectra where the intensity of the sodium peak was less than 1% of the total spectral intensity were used. The

mass scales of the positive and negative ion ToF-SIMS spectra were calibrated to the CH_3^+, $C_2H_3^+$, $C_3H_5^+$, and $C_7H_7^+$ peaks and the CH^-, CN^-, and CNO^- peaks, respectively, before further analysis.

The data treatment followed the procedure reported previously. Since it is difficult to determine how the relative intensities of these peaks are related to surface chemistry, Principal Component Analysis (PCA) is useful to reduce the dimensionality of a large data set while retaining its original information. Suppose there are *m* ToF-SIMS spectra and *n* selected peaks in each spectrum, a data set can be written as a matrix **X** with *m* rows by *n* columns. This can also be visualized as *m* points in a *n*-dimensional space. Before PCA, the intensities of the selected peaks from a spectrum are normalized to their total intensities and then mean-centered. The purposes are to correct for the difference in total secondary ion yield and to center the data set at the origin so that the variance is due to the difference in sample variance instead of in sample mean. This will generate a normalized and mean-centered data set $\boldsymbol{X}$. From the eigenvectors and eigenvalues of its variance –covariance matrix, $\boldsymbol{X}$ can be reduced to the sum of a cross-product of two smaller matrixes **P** and **T** and a residual matrix **E**: $\boldsymbol{X} = \mathbf{PT}^T + \mathbf{E}$, where **P** is the matrix of scores and **T** is the matrix of eigenvectors, called loadings. The residual matrix **E** represents noise. Matrix rotation in PCA creates a new set of axes (principal components, PCs) that define the directions of major variations within the data set. For example, PC1 defines the direction of the greatest variance while PC2 is the orthogonal axis that defines the direction of the next greatest variance not explained in PC1. The loadings generated are the direction cosines of this matrix rotation, describing the relationship between the original variables and the new PC axes. The scores are a projection of the samples onto the new PC axes, describing the relationship among the samples in the new axis system. A large data set is then reduced to a few variables (PCs), making the detection of patterns in the data set more straightforward. PCA was done using PLS Toolbox v. 2.0 (Eigenvector Research, Manson, WA) for MATLAB (the MathWorks Inc., Natick, MA). The PCA model was built using the data from the reference samples, i.e. adsorbed $F(ab')_2$ and Fc fragments. The data from adsorbed anti-hCGs on different substrates were projected into this PCA model to obtain their scores.

DNA-Directed Protein Immobilization via OEG and ssDNA SAMs: Mixed ssDNA/OEG SAMs were formed by immersing clean Au chips in a 1.0M KH_2PO_4 buffer solution of ssDNA and OEG thiols. The ssDNA thiol concentration was held constant at 100 nM for all experiments, while the OEG thiol concentration ranged from 0 – 100 μM. All SPR experiments began with a buffer baseline (TE-NaCl: 10 mM Tris-HCl with 1 mM EDTA, NaCl concentration as indicated, pH 7.2) and buffer was run again between each protein or DNA step. Solutions were flowed at a rate of 50 μl/min. Antibody conjugate and

secondary antibody solutions were prepared at 0.02 and 0.05 mg/ml, respectively. For the surface optimization experiments the antigen concentration was 1.0 μg/ml. For the hCG detection experiments, 1mg/ml Bovine Serum Albumin (BSA) was added to the buffer to minimize protein losses due to protein degradation and non-specific adsorption to tubing.

DNA-Directed Protein Immobilization SAMs via a Streptavidin Bridge: A mixture of OEG alkyl thiol and biotinylated alkyl thiol (BAT) was dissolved in absolute ethanol. The BAT, a C15 alkanethiol chain linked to a biotin head group by three ethylene glycol groups, was used as the specific binding element of the SAM, targeting streptavidin, while the OEG, a C10 alkanethiol chain linked to a hydroxyl head group by four ethylene glycol groups, created a non-fouling background.

SPR sensor chips, BK7 glass chips 32 mm x 15 mm x 1.5 mm, were coated with 2 nm of Cr and 48 nm of Au by electron beam evaporation. The cleaned chips were immersed in the OEG/BAT solution described. A sensor chip was mounted into a home-built SPR sensor. Streptavidin in a Tris-EDTA (TE) (10 mM Tris, 1 mM EDTA, pH 7.4) with 1 mg/mL BSA solution was flowed in both chambers at a concentration of 0.05 mg/mL. Biotinylated single-stranded oligonucleotides (bDNA) were immobilized on the layer of streptavidin. Custom oligonucleotides were modified with a 5' end attachment of a C6 linker and a biotin molecule. Two different sequences of DNA were used. Sequence A or B was flowed into one of the flow channels at a concentration of 100 nM in TE buffer with 1 mg/mL BSA for 10 minutes. This created a distinct DNA spot on the sensor surface. Antibody-DNA conjugates were immobilized onto the sensor surface by making use of the specificity of DNA hybridization. Antibody-DNA conjugates were flowed in the SPR flow channels at a concentration of 0.02 mg/mL in a TE buffer (10 mM Tris, 1 mM EDTA, pH 7.4) with 1 mg/mL BSA for 30 minutes.

Results and Discussion

In this work, MC simulations were performed to study the orientation of a model protein under a wide range of conditions using the 12-bead model (part 1) and the orientation of IgG1 and IgG2a using the residue-model (part 2). MD simulations were performed to study protein conformation in the presence of explicit water molecules and ions. Since IgG1 or IgG2a is too large for MD simulations with explicit atomic models, cytochrome c was studied instead (part 3). In order to control protein orientation, we proposed a charge-driven protein orientation principle. In this work, NH2 and COOH SAMs were used to model positively and negatively charged surfaces, respectively. IgG1 (large dipole) and IgG2a (small dipole) are used as model proteins. SPR is used to probe antigen response to the immobilized antibody. If the immobilized antibody has a desirable orientation, then antigen

response should be high. While SPR detection is an indirect way to probe protein orientation (part 4), ToF-SIMS is used to probe protein orientation directly (part 5).

To create protein arrays, the ssDNA probe surface was a mixed SAM of ssDNA and OEG terminated thiols (part 6) or the sensor platform was based on biotinylated single-stranded DNA immobilized via a streptavidin bridge to a mixed SAM of biotinylated alkanethiol and OEG (part 7).

1. Predicting Protein Orientation Based on a 12-Bead Model

Generally, it is found that the isoelectric point (IEP) (the net charge of a protein is zero at this pH value) of $(F_{ab})_2$ fragment is larger than that of whole antibody, while the IEP of F_c fragment is smaller than that of whole antibody. Therefore, at the IEP of the whole antibody, the $(F_{ab})_2$ fragment will carry positive charge while the F_c fragment will carry negative charge. Therefore, the whole antibody molecule will have a dipole pointing from F_c to $(F_{ab})_2$ fragment. Our dipole calculation for all-atom IgG1 also verifies this. Based on this property of a protein, it is feasible to control protein orientation on charged surfaces by tuning surface and solution conditions. The effects of different charged surfaces, pH value of a solution, colloidal model antibodies with different dipole moments, surface charge density, and solution ionic strength on the orientation of adsorbed antibody on charged surfaces are investigated in this work.

The orientation angle distribution function is used to characterize the orientation of the antibody on different surfaces. The orientation angle of an adsorbed antibody molecule is defined as the angle between the unit vector normal to the surface and the unit vector along the dipole of antibody. The cosine of the orientation angle, $\cos\theta$ of 1, represents an "end-on" (F_c closer to surface) orientation; -1, a "head-on" (F_{ab} closer to surface) orientation; and 0, a "lying-flat" (both F_{ab} and F_c closer to surface) orientation. An illustration is shown in **Figure 1.1**.

A. Twelve-bead simulations

Effect of charged surfaces: The effect of different charged (positive, neutral and negative) surfaces on the orientation of adsorbed model antibodies is shown in **Figure 1.2**. On the positively charged surface, the desired "end-on" orientation is obtained because of attraction between the F_c fragment and the surface and repulsion between the F_{ab} fragments and the surface. **Figure 1.3** shows the distribution of distance to the surface for F_c and F_{ab} fragments on a positively charged surface. F_c fragment closer to the surface indicates an "end-on" orientation. The antibody has "head-on" orientation on the negatively charged surface and "lying-flat" orientation on the neutral surface. Lu et al. [11] found that the

dispersion (VDW) attraction played a major role in protein adsorption on neutral polymer surfaces, which agrees with our finding. From our simulation predictions, it is expected that antigen response to adsorbed antibody will follow the order of positively charged surface > neutral surface > negatively charged surface. Antibody orientation is mainly responsible for the difference in antigen response to adsorbed antibody. It was found in the work by Buijs et al. [1] that antigen response is higher for antibody adsorbed on methylated surface (neutral surface) than on silicon surface (negatively charged surface). Our simulation predictions are consistent to the experimental results.

Based on our hypothesis of charge-driven protein orientation and theoretical predictions using the proposed simple antibody model, we performed experimental studies of antibody adsorption on positively charged NH_2-terminated SAMs and negatively charged COOH-terminated SAMs. Our SPR biosensor experiments verify that antigen response is higher on NH_2-terminated SAMs than on COOH-terminated SAMs. Our ToF-SIMS results show that antibody orientation turns out to be "end-on" on NH_2-terminated SAMs and "head-on" on COOH-terminated SAMs.

Effect of antibody dipole moment: Table 1.1 summarizes results on the orientations of three model antibodies (antibodies 1, 2 and 3) with different dipole moments adsorbed on a positively charged surface with $\sigma_s = 0.0045 C/m^2$ and I = 0.015M under three different pH values – below IEP (case a), at IEP (case b), and above IEP (case c). As solution pH changes, the net charge of these antibodies will vary – positive below IEP (case a), zero at IEP (case b), and negative above IEP (case c). For each pH value, three different model antibodies with different dipole moments are studied. It should be pointed out that the net charge and the dipole moment of an antibody are not independent variables. Varying pH will affect both net charge and dipole moment for a specific antibody of interest. If a specific antibody with available explicit molecular structure is studied, then one should be able to calculate both net charges and dipoles of this antibody at different pH values. The 12-bead model, which is simplified from the Y-shape of antibody structure, is used with an objective to quickly map out the effect of various factors on protein orientation of various antibodies. Thus, we select three net charges (cases a, b, and c) to represent different pH values and three dipole moments (antibodies 1, 2, and 3) to represent three antibodies for each pH value.

It can be found from **Table 1.1** that at the IEP of model antibodies, the stronger the dipole moment of a model antibody, the more the desired "end-on" orientation (see cases b1, b2, and b3). For the antibody with smaller dipole moment (case b1), VDW interactions dominate. The model antibody tends to lie on the surface. For the antibodies with relatively larger dipole moments (cases b2 and b3), electrostatic interactions dominate. These antibodies have "end-on" orientation on the positively charged surface. When the pH value

of solution is below the IEP, the antibody with smaller dipole moment (case a1) will have "lying-flat" orientation, while the antibodies with larger dipole moments (cases a2 and a3) will have "end-on" orientation. For cases a2 and a3, though "end-on" orientations are obtained, since the net charge of the antibody is positive and the surface is positively charged, this leads to higher antibody adsorption energy and weaker adsorption as shown in **Table 1.1**, which is not favorable for practical applications. As Noinville et al. [9] pointed out, the net charge of protein was an important factor for adsorption. When the pH value of solution is above the IEP, antibodies with smaller dipole moments (cases c1 and c2) will have "lying-flat" orientations. Only the antibody with larger dipole moment (case c3) will have the desired "end-on" orientation.

It can be seen that the orientation of adsorbed antibody results from the compromise between VDW and electrostatic interactions. When electrostatic interactions dominate, the dipole moment of an antibody is an essential factor for its orientation on charged surfaces. The pH value of solution plays an important role to determine antibody orientation and adsorbed amount through its influence on the dipole moment and net charge of the antibody. Juffer et al. found that close to the surface, the mean force acting on protein clearly varied with the strength of the dipole moment, and suggested that a correlation between the dipole and the protein orientation with respect to the surface could be established. In their work, only electrostatic interactions were considered. We also calculated the orientation and adsorption interaction energies of adsorbed model antibodies on a positively charged surface with higher surface charge density of $\sigma_s = 0.018 C/m^2$ at I = 0.015M. For cases b1, b2, and b3, the "end-on" orientation is always found since surface charge density is now four times higher and electrostatic interactions dominate for these three cases. This indicates that for antibodies with smaller dipole moments, desired orientation could still be achieved on surfaces with higher surface charge density.

Effect of surface charge density and solution ionic strength: We also investigated the effect of surface charge density and solution ionic strength on the orientation of adsorbed antibodies on positively charged surfaces. Results are presented in **Figure 1-4**. At four different solution ionic strengths, with the increase of surface charge density, more antibodies with the desired "end-on" orientation are obtained due to stronger protein-surface interactions. Thus, high surface charge density favours the desired "end-on" orientation of the studied model antibody on positively charged surfaces. For positively charged surfaces with the same surface charge density, it can be seen that the smaller the solution ionic strength, the more the "end-on" orientation. It is well known that the electrostatic interactions are the driving force in ion-exchange chromatography and protein adsorption. In

this study, it was found that electrostatic interaction also plays an important role in determining the orientation of adsorbed antibodies. At high ionic strength, electrostatic interactions are screened, leading to the "lying-flat" orientation. At low ionic strength, electrostatic interactions are the dominant factor in controlling the adsorption and orientation of antibody. Roth and Lenhoff [15] found that stronger electrostatic interactions enhance the adsorbed amount of proteins and such an enhancement is most pronounced at low ionic strength. Similarly, as shown in this work, stronger electrostatic interactions enhance the orientation of adsorbed antibodies. Thus, low ionic strength favours the desired "end-on" orientation of the model antibody on positively charged surfaces. The snapshots of the adsorbed antibody layer on a positively charged surface of $\sigma_s = 0.012 C/m^2$ are shown in **Figure 1.5** for two solutions with different ionic strengths. It can be seen that most model antibodies have "end-on" orientation (side view of **Figure 1.5c**) at a low solution ionic strength of 0.015M, while most antibody molecules have "lying-flat" orientation (top view of **Figure 1.5b**) at a high solution ionic strength of 0.1M.

At the initial stage of this work, the orientation of only one model antibody molecule was studied. This corresponds to low surface coverage. To obtain better statistics and consider the effect of protein-protein interactions, molecular simulations at high surface coverage were performed. Calculations indicate that protein-protein interactions are 100 times less important than protein-surface interactions for the system studied in this work. Because of this, protein-protein interactions do not significantly affect protein orientation even at high surface coverage. Thus, antibody orientation is not significantly affected by antibody surface coverage. In fact, predicted antibody orientation is quite similar regardless of low or high-surface coverage used in this work. As discussed before, protein-protein interactions are much weaker than protein-surface interactions. Thus, after the formation of the first adsorbed protein layer, it is not expected that a second protein layer will form. Simulation results show that there is no multi-layer adsorption and antibody stacking. Due to the non-spherical shape of an antibody molecule, antibody orientation will determine antibody surface coverage. At high surface charge density and low ionic strength when electrostatic interaction dominates, the model antibody will have "end-on" orientation on positively charged surfaces and "head-on" orientation on negatively charged surfaces. "End-on" or "head-on" orientations will lead to higher surface coverage due to the aspect ratio of an antibody molecule. At low surface charge density and high ionic strength when van der Waals interaction dominates, the model antibody will have "lying-flat" orientation, for which each molecule occupies larger surface area than it does for "end-on" orientation. Thus, lower surface coverage is expected. As shown in **Figure 1.5**, surface coverage at an ionic strength of 0.1M ("lying-flat" orientation) is lower than that at 0.015M ("end-on" orientation).

B. All-atom simulations

The orientation of an all-atom antibody molecule on positively or negatively charged surfaces (+/- 0.037C/m^2) was also investigated at 0.005M by MC simulations. For all-atom simulations, the atomistic structure is from the protein databank; whereas the partial charge of each atom is from the CHARMM force field. The results are shown in **Figure 1.6**. It is obvious that the "end-on" orientation is obtained on the positively charged surface with orientation angle $\cos\theta$ =0.82 (**Figure 1.6a**). Deviation to 1.0 is due to the non-flat shape of the patch of IgG1 near the surface and a compromise between VDW and electrostatic interactions. The "head-on" orientation is achieved on the negatively charged surface with orientation angle $\cos\theta$ =-0.98 (**Figure 1-6b**). Simulation results based on a 12-bead colloidal model are consistent with those based on an all-atom model. Simulations based on both colloidal and all-atom models show that the desired IgG1 orientation is achieved on positively charged surfaces at low ionic strength, important for biosensor applications. Though it is intuitional that the charge distribution of a protein may determine its final orientation on charged surfaces, the importance of the dipole of a protein for the control of protein orientation is seldom addressed.

From the discussion of simulation results by colloidal model, it is seen that the stronger dipole protein molecule may have a more controlled orientation on charged surfaces. Based on the direction of the dipole of the antibody molecule, if there are more negatively charged residues in the F_c fragment of the antibody molecule, then, one may obtain more ordered orientation of IgG1 on positively surface. One can further use the site-directed mutagenesis technique to get mutants of IgG1, then, using the mutants to get better-controlled orientation for sensor applications, since the electrostatic interaction energy of residues proximal to a surface is larger than those of far away from a surface. To get a stronger dipole in an antibody, one could mutate those positively charged and neutral residues close to surface to negatively charged residues GLU or ASP. From the all-atom simulation, one finds the following residues near surface, B chain of IgG1's F_c fragment, Lys281, Pro308, Arg309, Gln312, Phe313, Asn314, Ser317, Lys385; D chain of IgG1's F_c fragment, Thr428. For biosensor applications, it is expected to result in better-controlled "end-on" orientation on positively charged surfaces by site-directed mutagenesis of these residues to negatively charged residues.

Table 1.1 Orientation and interaction energies between a positively charged surface of $\sigma_s = 0.0045 C/m^2$ and three model antibodies at an ionic strength of 0.015M below (case a), at (case b), or above (case c) IEP.

case	pH	dipole (D)	$Q(F_{ab})$ (e)	$Q(F_c)$ (e)	U_{tot} (kJ/mol)	U_{VDW} (kJ/mol)	U_{elec} (kJ/mol)	orientation
a1	<IEP	368	2	0	-8.235	-12.326	4.091	Lying-flat
a2	<IEP	1207	4	-2	-4.875	-1.303	-3.572	End-on
a3	<IEP	2046	6	-4	-9.415	-1.628	-7.787	End-on
b1	=IEP	839	2	-2	-12.414	-12.406	-0.008	Lying-flat
b2	=IEP	1679	4	-4	-9.450	-1.629	-7.821	End-on
b3	=IEP	2518	6	-6	-13.758	-1.802	-11.956	End-on
c1	>IEP	472	0	-2	-16.599	-12.497	-4.102	Lying-flat
c2	>IEP	1311	2	-4	-16.605	-12.481	-4.124	Lying-flat
c3	>IEP	2150	4	-6	-13.752	-1.800	-11.952	End-on

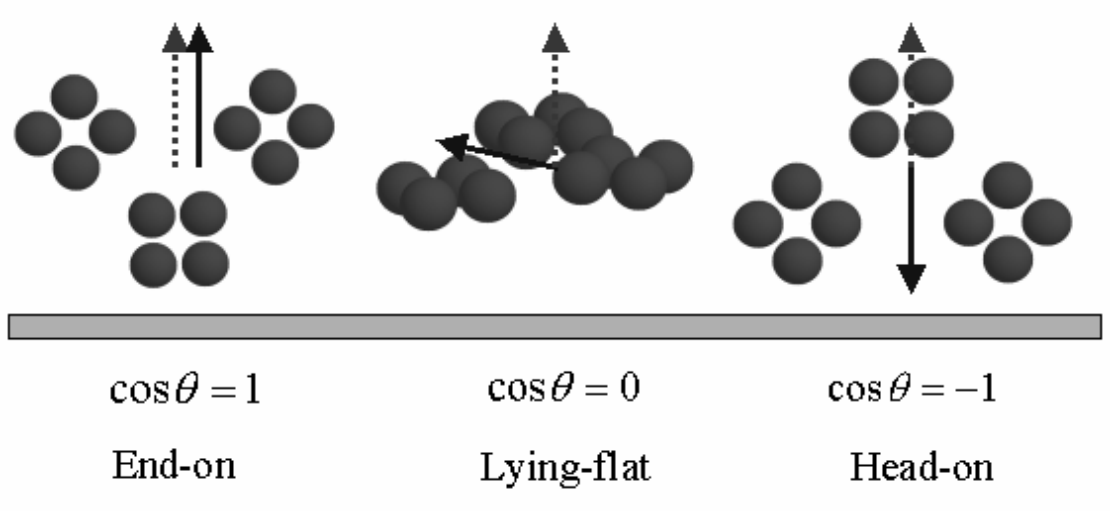

Figure 1.1 Definition of the orientation of adsorbed antibody. The solid arrow denotes the unit vector along the dipole of antibody whereas the dashed arrow represents the unit vector normal to the surface.

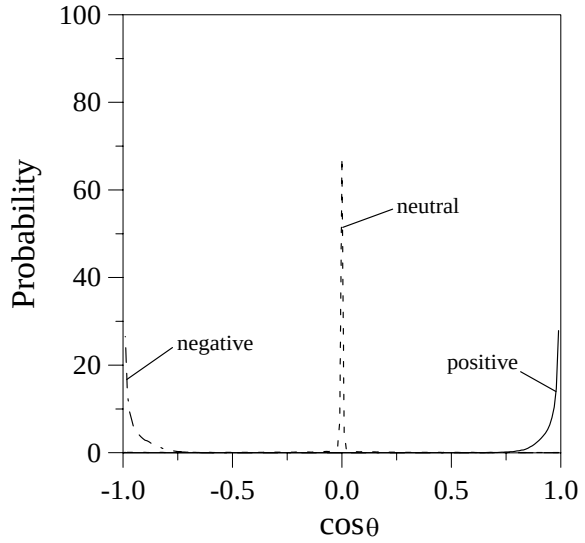

Figure 1.2 Effect of surface charge sign on the orientation of the adsorbed model antibody with a dipole moment of 1679D at an ionic strength of 0.015M on a positively charged surface $\sigma_s = 0.018 C/m^2$ (solid line), a neutral surface $\sigma_s = 0.0 C/m^2$ (dashed line), and a negatively charged surface $\sigma_s = -0.018 C/m^2$ (dot dashed line).

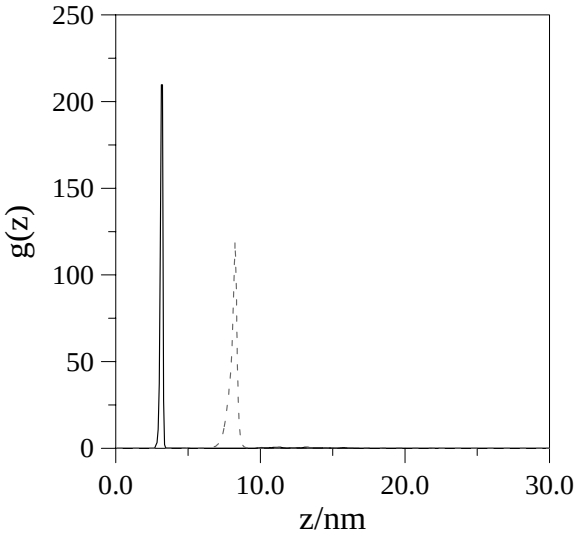

Figure 1.3 Distance distribution of Fab (dashed line) and Fc (solid line) fragments for the case of the positively charged surface.

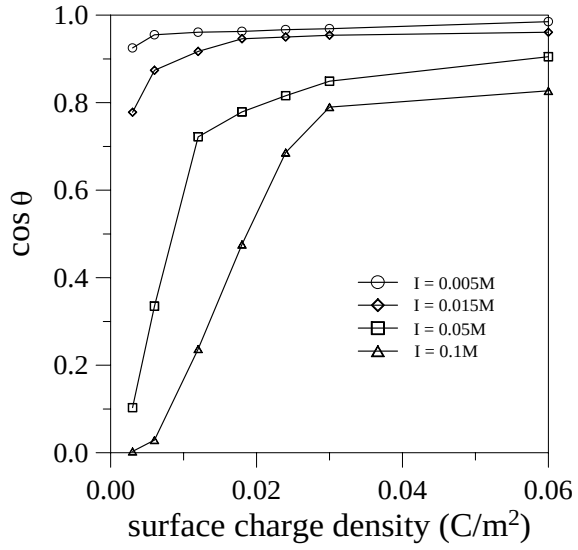

Figure 1.4 Effect of surface charge density and solution ionic strength on the orientation of the adsorbed model antibody with a dipole moment of 1679D on positively charged surfaces.

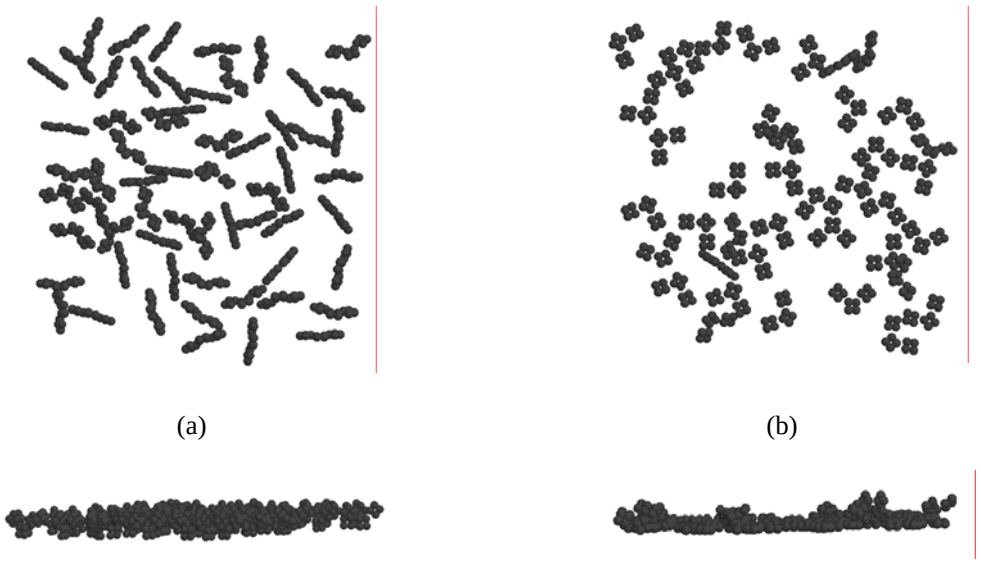

(a) (b)

(c) (d)

Figure 1.5 Snapshots of adsorbed model antibodies on a positively charged surface of $\sigma_s = 0.012C/m^2$ at an ionic strength of 0.015M (a, c) and 0.1M (b, d). Top view, a and b; Side view, c and d.

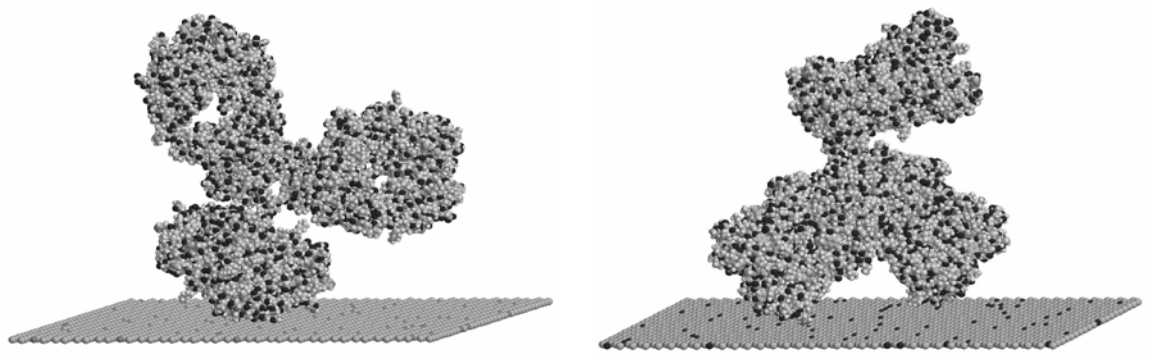

(a) (b)

Figure 1.6 Configurations of adsorbed all-atom antibodies on charged surfaces at an ionic strength of 0.005M. (a), on a positively charged surface; dark dots on the surface are positively charged atoms. (b), on a negatively charged surface; dark dots on the surface are negatively charged atoms.

2. Predicting Protein Orientation Based on a Residue Model

The adsorption and orientation of IgG1 and IgG2a on both positively charged and negatively charged surfaces are studied by MC simulations. The orientation angle is used to quantitatively characterize the orientation of the two antibodies on different charged surfaces. The orientation angle of an adsorbed antibody molecule is defined as the angle between the unit vector normal to the surface and the unit vector along the dipole of an antibody. Adsorption energies and average values of the cosine of orientation angles of IgG1 and IgG2a at different surface and solution conditions are shown in **Tables 2.1-2.4**. The configurations of the two antibodies on positively and negatively charged surfaces are shown in **Figures 2.1 – 2.4**. In **Figures 2.1-2.4**, the two red circles in each configuration indicate the two antigen-antibody binding sites. In **Tables 2.1-2.4**, at each condition, there is a lowest-energy orientation, which is most favorable. Roush et al. [10] calculated the interaction energy of rat cytochrome b5 on an anion-exchange adsorbent surface at discrete separation distances and orientations. Their results revealed the presence of a preferred orientation. In other studies, it was also found that protein-surface interaction energy was dependent on protein orientation on the polymer surfaces.

At some conditions, there exist multiple orientations for both IgG1 and IgG2a. The relationship between the probability of a specific configuration and its energy is

$$P_i = \frac{\exp(-U_i/kT)}{\sum_i \exp(-U_i/kT)}$$

where U_i is the adsorption energy of configuration *i*, k is the Boltzmann constant, and T is the temperature. At 298K, $1kT$ corresponds to $2.48kJ \cdot mol^{-1}$. Any configuration, whose adsorption energy is $17.1kJ \cdot mol^{-1}$ higher than the lowest one, will be discarded, since the probability of appearance for this orientation will be less than 0.1%.

IgG1 on positively charged surfaces. From **Table 2.1** and **Figure 2.1**, it can be seen that at low ionic strengths, 0.005M and 0.015M, IgG1 on positively charged surface has a typical "end-on" orientation as shown in **Figure 2.1a**. At high ionic strengths, 0.1M and 0.3M, IgG1 on positively charged surface mainly exhibits another "end-on" orientation as shown in **Figure 2.1b**. The orientation shown in **Figure 2.1b** is very similar to that in **Figure 2.1a**, but with 9^o smaller orientation angle. The "lying" orientation shown in **Figure 2.1c** only appears at high ionic strength 0.3M and low surface charge density $0.006 C \cdot m^{-2}$. Under this condition, VDW interactions dominate and the behavior of adsorbed antibodies is similar to that on a neutral surface. Lu and Park [11] found that dispersion (VDW) attraction played a major role in protein adsorption on neutral polymer surfaces, which is consistent

with our finding. Usually, IgG1 will have an "end-on" orientation on positively charged surfaces when electrostatic interactions dominate. This indicates that adsorbed IgG1 on positively charged surfaces is well suited for biosensor applications.

IgG1 on negatively charged surfaces. From **Table 2.2** and **Figure 2.2**, it can be seen that at low ionic strengths, 0.005M and 0.015M, IgG1 has a "head-on" orientation on a negatively charged surface as shown in **Figure 2.2a**. The negatively charged surface repels the F_c fragment and attracts the F_{ab} fragments. This indicates that antigen response should be very low since binding sites are not accessible to antigens when adsorbed antibody has a "head-on" orientation. Buijs et al. [1] studied antigen response using adsorbed antibody on a negatively charged silicon surface, and found that the antigen response was low. At high ionic strengths, 0.1M and 0.3M, IgG1 has a "side-on" orientation as shown in **Figure 2.2b**, with one of the Fab fragments on the surface. At low surface charge density of $-0.006\,C\cdot m^{-2}$ and high ionic strength 0.3M where VDW interactions dominate, IgG1 exhibits a "lying" orientation as shown in **Figure 2.2c**.

From simulation results in this study for IgG1 on positively and negatively charged surfaces, it is expected that IgG1 adsorbed on positively charged surface would show higher antigen response than on a negatively charged surface. Recent experiments from SPR biosensor verify that IgG1 adsorbed on positively charged amino-terminated SAMs shows higher antigen response than on negatively charged carboxyl-terminated SAMs at low ionic strengths. ToF-SIMS results also show the tendency of the "head-on" orientation of IgG1 on carboxyl-terminated SAM and the "end-on" orientation of IgG1 on amino-terminated SAM, which agrees well with the simulation prediction.

IgG2a on positively charged surfaces. From **Table 2.3** and **Figure 2.3**, at a surface charge density of $0.018\,C\cdot m^{-2}$, when ionic strengths is low as 0.005M and 0.015M, IgG2a shows "end-on" orientations as **Figure 2.3a** and **Figure 2.3b**, respectively. Configurations **Figure 2.3a** and **Figure 2.3b** are similar except that the orientation angle of **Figure 2.3a** is 20^o closer to the vector perpendicular to the surface than that of **Figure 2.3b**, due to larger electrostatic interactions. At low ionic strength of 0.005M, when surface charge density is $0.006\,C\cdot m^{-2}$, IgG2a shows a "slanting" orientation **Figure 2.3c**, with the F_c fragment and one F_{ab} fragment on the positively charged surface. The direction of the dipole of IgG2a is pointing from F_c fragment to another F_{ab} fragment. At the same ionic strength of 0.005M, IgG2a displays orientations **Figure 2.3c** and **Figure 2.3a** respectively on 0.006 and $0.018\,C\cdot m^{-2}$ surfaces; because stronger electrostatic interactions (due to higher surface charge density) will repel the F_{ab} fragments more away from the surface. For the same reason, at the same ionic strength of 0.015M, IgG2a shows different preferred orientations as **Figure 2.3c** and **Figure 2.3b** on 0.006 and $0.018\,C\cdot m^{-2}$ surfaces.

At high solution ionic strengths, 0.1M and 0.3M, VDW interactions dominate. IgG2a has "lying" orientations on positively charged surfaces, as shown in **Figures 2.3d**, **2.3e** and **2.3f**. At low ionic strength 0.015M and low surface charge density $0.006\,C\cdot m^{-2}$, IgG2a also shows a "lying" orientation, since VDW interactions dominate at this condition. Configurations shown in **Figures 2.3d** and **2.3f** are very similar to each other except that different F_{ab} fragments are closer to the surface. Configurations shown in **Figures 2.3e** and **2.3f** are both "lying" orientations, but with opposite sides of IgG2a facing to the surface.

IgG2a on negatively charged surfaces. From **Table 2.4** and **Figure 2.4**, it can be seen that at low ionic strength of 0.005M and surface charge density of -0.006 or -0.018 $C\cdot m^{-2}$, or at 0.015M and -0.018 $C\cdot m^{-2}$ condition, IgG2a shows a "side-on" orientation (**Figure 2.4a**), with one F_{ab} fragment on the surface and another F_{ab} fragment pointing outward from the surface. Under these conditions, electrostatic interaction plays an important role. It is expected that there should be some antigen response for IgG2a adsorbed on a negatively charged surface. Recent SPR experiments show that antigen response for IgG2a on carboxyl-terminated SAMs is comparable to that on amino-terminated SAMs. At ionic strength of 0.015M and surface charge density of -0.006 $C\cdot m^{-2}$, IgG2a displays a "head-on" orientation as shown in **Figure 2.4b**, since the electrostatic interaction of orientation **Figure 2.4b** is not as strong as that of orientation **Figure 2.4a**. At high ionic strengths 0.1M and 0.3M where VDW interactions dominate, IgG2a has multiple orientations as shown in **Figures. 2.4c**, **2.4d**, and **2.4e**.

Comparing the orientations of IgG1 and IgG2a at the same condition, IgG1 has less orientation than IgG2a has on both positively and negatively charged surfaces. This is due to the larger dipole moment of IgG1 than that of IgG2a. Juffer et al. [12] found that close to the surface the mean force acting on the protein clearly varied with the strength of the dipole moment, and suggested a correlation between the dipole and the protein orientation with respect to the surface. However, only electrostatic interaction was considered in their work; this corresponds to the situation when electrostatic interactions dominate in this work. Ramsden et al. [31] studied the adsorption of two mutants of cytochrome b5. They found that E15Q adsorbs with its major axis perpendicular to the surface, while E48Q has a more flexible adsorption mode due to the larger dipole moment of E15Q. **Figure 2.5**, shows the orientation distribution of IgG1 and IgG2a at 0.005M and $0.018\,C\cdot m^{-2}$. It is obvious that IgG1 exhibits a narrower distribution for specific orientation than IgG2a does at the same solution and surface condition, which is still due to the larger dipole moment of IgG1 than that of IgG2a.

It is well known that electrostatic interaction plays an important role in ion-exchange chromatography, and protein adsorption. Ball et al. [13] measured the adsorption kinetics of

lysozyme on a Si(Ti)O_2 surface. They found that the increases in adsorbed amount was linear with time at low ionic strength 0.01M, while the linear regime was not observed at high ionic strength 0.15M, suggesting an electrostatically driven self-assembled process at low ionic strength. This indicates that the adsorption kinetics of lysozyme is ionic strength-dependent. Ben-Tal et al. [14] found that the binding energy of small basic peptides to membranes decreases as salt concentration increases. Roth and Lenhoff [15] found that stronger electrostatic interactions enhanced the adsorbed amount of proteins and such an enhancement was most pronounced at low ionic strength. This work shows the similar trend of the influence of electrostatic interaction on the orientation of adsorbed antibodies; it was found that the orientation of adsorbed antibodies is also ionic strength-dependent. For both IgG1 and IgG2a, at low ionic strength and high surface charge density conditions, preferred orientations are observed, since electrostatic interactions dominate. While at high ionic strength and low surface charge density conditions, multiple orientations were observed, since VDW interactions dominate. For both IgG1 and IgG2a, some orientations appear on both positively and negatively charged surfaces. For these cases, usually VDW interactions dominate. San Paulo and Garcia [16] obtained several high-resolution images of antibodies on mica using tapping-mode atomic force microscopy and found several morphologies, including “end-on”, “head-on”, “side-on” and “lying”. They consider this phenomenon as a consequence of the nonspecific adhesion of antibodies on mica. Since mica surface is weakly charged, electrostatic interaction is not strong and VDW interaction dominates, so multiple orientations are expected. This is in good agreement with predictions in this study.

Table 2.1 Energies and orientations of IgG1 on positively charged surfaces

σ_s	I	U	U_{VDW}	U_{ele}	$\langle\cos\theta\rangle$	orientation	Fig	P
$C \cdot m^{-2}$	M	$kJ \cdot mol^{-1}$	$kJ \cdot mol^{-1}$	$kJ \cdot mol^{-1}$				%
0.006	0.005	-354.1	-63.4	-290.7	0.86	End-on	2.2a	100.00
	0.015	-220.7	-59.9	-160.8	0.86	End-on	2.2a	100.00
	0.1	-114.6	-78.5	-36.1	0.77	End-on	2.2b	100.00
	0.3	-92.0	-78.0	-14.0	0.77	End-on	2.2b	97.97
		-82.4	-80.6	-1.8	0.03	Lying	2.2c	2.03
0.018	0.005	-948.0	-58.7	-889.3	0.86	End-on	2.2a	100.00
	0.015	-537.7	-53.5	-484.2	0.86	End-on	2.2a	100.00
	0.1	-187.8	-78.1	-109.7	0.77	End-on	2.2b	100.00
	0.3	-120.3	-78.5	-41.8	0.77	End-on	2.2b	100.00

Table 2.2 Energies and orientations of IgG1 on negatively charged surfaces

σ_s	I	U	U_{VDW}	U_{ele}	$\langle\cos\theta\rangle$	orientation	Fig	P
$C \cdot m^{-2}$	M	$kJ \cdot mol^{-1}$	$kJ \cdot mol^{-1}$	$kJ \cdot mol^{-1}$				%
-0.006	0.005	-295.9	-51.7	-244.2	-0.98	Head-on	3a	100.00
	0.015	-159.1	-51.1	-108.0	-0.98	Head-on	3a	100.00
	0.1	-79.6	-60.7	-18.9	-0.21	Side-on	3b	98.88
		-68.5	-73.0	4.5	0.03	Lying	3c	1.12
	0.3	-71.6	-73.3	1.7	0.03	Lying	3c	91.54
		-65.7	-60.4	-5.3	-0.22	Side-on	3b	8.46
-0.018	0.005	-784.3	-51.4	-732.9	-0.98	Head-on	3a	100.00
	0.015	-376.1	-50.6	-325.5	-0.98	Head-on	3a	100.00
	0.1	-117.2	-61.1	-56.1	-0.21	Side-on	3b	100.00
	0.3	-76.6	-60.0	-16.6	-0.21	Side-on	3b	97.52
		-67.5	-72.6	5.1	0.03	Lying	3c	2.48

Table 2.3 Energies and orientations of IgG2a on positively charged surfaces

σ_s	I	U	U_{VDW}	U_{ele}	$\langle\cos\theta\rangle$	orientation	Fig	P
$C \cdot m^{-2}$	M	$kJ \cdot mol^{-1}$	$kJ \cdot mol^{-1}$	$kJ \cdot mol^{-1}$				%
0.006	0.005	-141.1	-90.3	-50.8	0.92	Slanting	4c	92.97
		-134.7	-82.7	-52.0	0.38	Lying	4d	7.03
	0.015	-108.3	-82.5	-25.8	0.38	Lying	4d	99.34
		-94.4	-90.3	-4.1	0.92	Slanting	4c	0.36
		-93.9	-80.8	-13.1	0.00	Lying	4e	0.30
	0.1	-89.3	-88.4	-0.9	-0.10	Lying	4f	54.94
		-87.5	-82.7	-4.8	0.38	Lying	4d	26.57
		-86.4	-80.9	-5.5	0.00	Lying	4e	17.04
		-80.3	-90.3	10.0	0.92	Slanting	4c	1.45
	0.3	-93.7	-91.3	-2.4	-0.12	Lying	4f	92.91
		-85.6	-82.9	-2.7	0.38	Lying	4d	3.53
		-84.7	-90.1	5.4	0.92	Slanting	4c	2.46
		-82.7	-80.8	-1.9	0.00	Lying	4e	1.10
0.018	0.005	-255.2	-40.3	-214.9	0.77	End-on	4a	99.36
		-242.7	-90.5	-152.5	0.92	Slanting	4c	0.64
	0.015	-160.3	-42.3	-118.0	0.52	End-on	4b	58.00
		-159.5	-81.0	-78.5	0.38	Lying	4d	42.00
	0.1	-97.4	-81.0	-16.4	0.00	Lying	4e	50.61
		-96.8	-82.1	-14.7	0.38	Lying	4d	39.72
		-93.3	-83.7	-9.6	-0.08	Lying	4f	9.67
	0.3	-97.7	-88.8	-8.9	-0.11	Lying	4f	92.97
		-90.9	-82.7	-8.2	0.38	Lying	4d	5.98
		-86.6	-80.9	-5.7	0.00	Lying	4e	1.05

Table 2.4 Energies and orientations of IgG2a on negatively charged surfaces

σ_s	I	U	U_{VDW}	U_{ele}	$\langle\cos\theta\rangle$	Orientation	Fig	P
$C \cdot m^{-2}$	M	$kJ \cdot mol^{-1}$	$kJ \cdot mol^{-1}$	$kJ \cdot mol^{-1}$				%
-0.006	0.005	-190.8	-58.1	-132.7	-0.94	Side-on	5a	100.00
	0.015	-131.0	-80.2	-50.8	-0.49	Head-on	5b	93.38
		-123.9	-57.6	-66.3	-0.94	Side-on	5a	5.32
		-120.4	-53.9	-66.5	-0.02	Slanting	5c	1.30
	0.1	-90.2	-80.2	-10.0	0.92	Slanting	5d	52.84
		-89.5	-87.4	-2.1	-0.13	Lying	5e	39.84
		-85.3	-79.3	-6.0	-0.48	Head-on	5b	7.32
	0.3	-85.4	-80.0	-5.4	0.92	Slanting	5d	55.83
		-84.6	-82.5	-2.1	-0.13	Lying	5e	40.43
		-78.7	-79.3	0.6	-0.48	Head-on	5b	3.74
-0.018	0.005	-456.3	-52.5	-403.8	-0.94	Side-on	5a	100.00
	0.015	-259.0	-57.4	-201.6	-0.94	Side-on	5a	91.54
		-253.1	-43.5	-209.6	-0.06	Slanting	5c	8.46
	0.1	-113.8	-55.0	-58.8	-0.02	Slanting	5c	80.41
		-110.3	-80.1	-30.2	0.92	Slanting	5d	19.59
	0.3	-95.8	-79.5	-16.3	0.92	Slanting	5d	99.61
		-81.3	-87.2	5.9	-0.14	Lying	5e	0.29

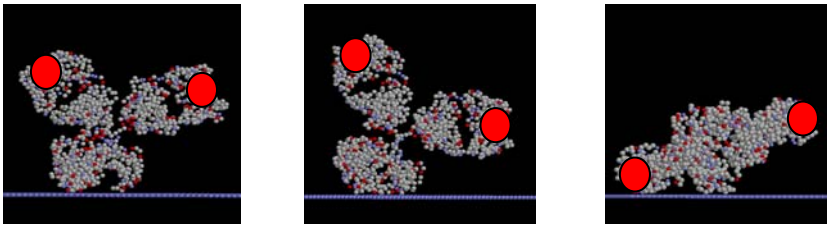

a B c

Figure 2.1 Typical orientations of IgG1 on positively charged surfaces.

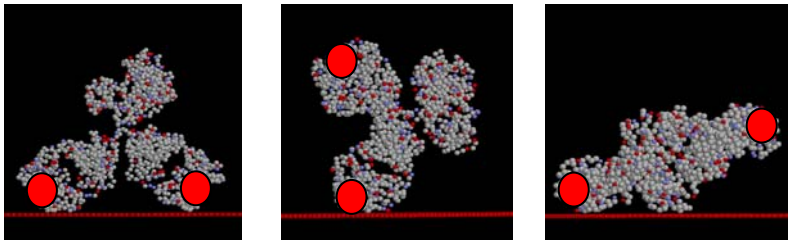

a b c

Figure 2.2 Typical orientations of IgG1 on negatively charged surfaces.

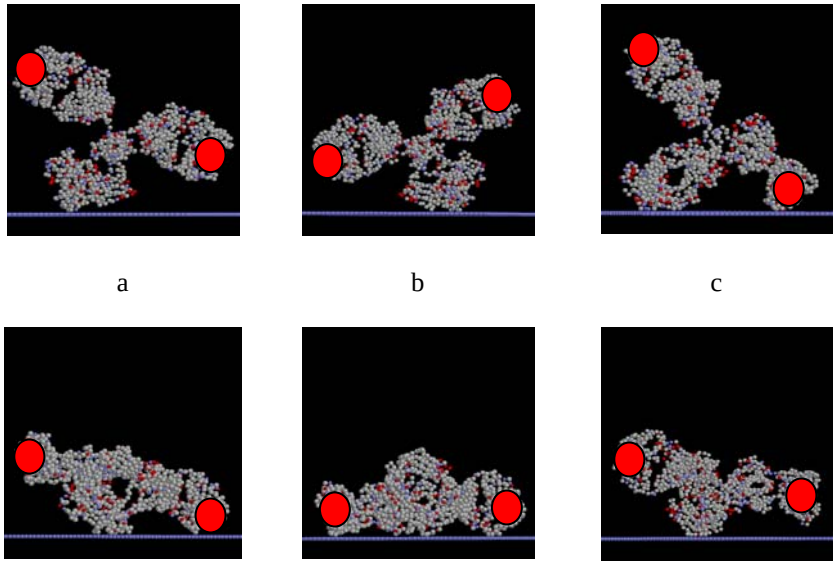

Figure 2.3 Typical orientations of IgG2a on positively charged surfaces.

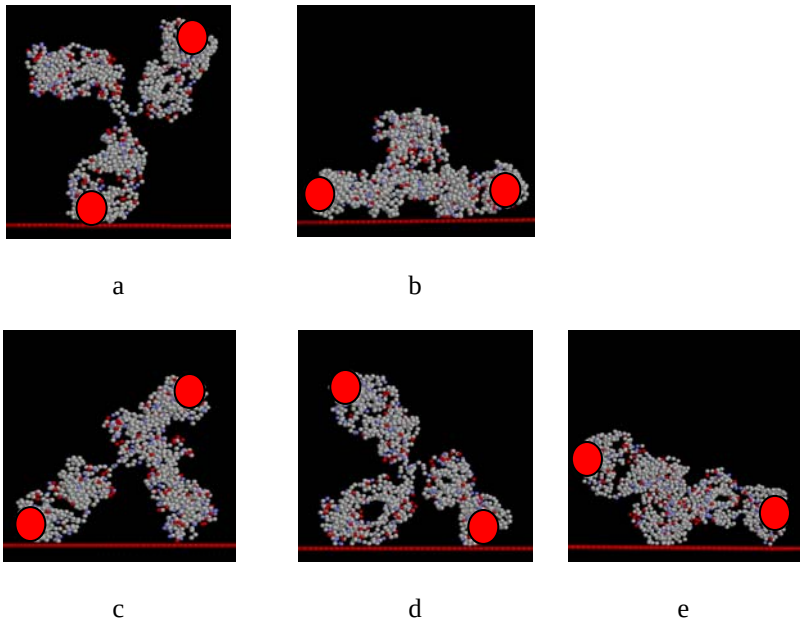

Figure 2.4 Typical orientations of IgG2a on negatively charged surfaces.

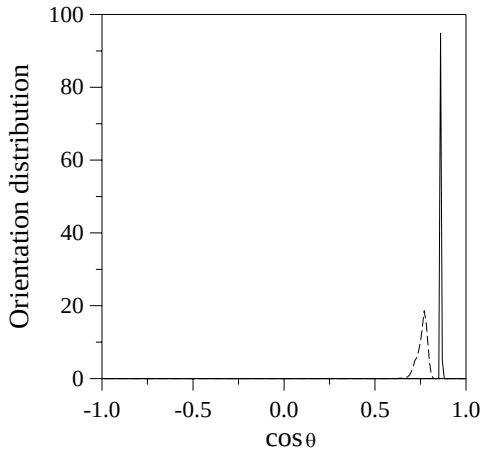

Figure 2.5 Orientation distributions of IgG1 and IgG2a on 0.018 $C \cdot m^{-2}$ positively charged surfaces at 0.005M. Solid line, IgG1; Dashed line, IgG2a.

3. Predicting Protein Conformation Based on an All-Atom Model

The orientation and conformation of Cyt-c on negatively charged carboxyl-SAMs with different dissociation degrees of 5%, 25%, and 50% were investigated by a combined MC and MD simulation approach. For comparison, Cyt-c behavior in the bulk solution was also studied. The preliminary orientation of Cyt-c on SAM surfaces was obtained from MC simulations. The optimal orientation, gyration radius, eccentricity, root mean square deviation (RMSD), superimposed structures, and dipole moment of Cyt-c were calculated during the MD simulations. Simulation results are summarized in **Table 3.1** and **Figures 3.1-3.7**. In **Table 3.1**, the reported results were averaged over 500ps after equilibration.

Orientation. The orientation angle is used to quantitatively characterize the orientation of Cyt-c on different surfaces. The orientation angle of the adsorbed Cyt-c molecule is defined as the angle between the unit vector normal to the surface and the unit vector along the dipole of Cyt-c. The cosine value of this angle is used to represent the orientation of adsorbed Cyt-c. The orientation distributions of Cyt-c on SAM surfaces are shown in **Figure 3.1**. Heme tilt angle is defined as the angle between the unit vector normal to the surface and the unit vector normal to the heme plane. From **Table 3.1** and **Figure 3.1**, it can be seen that there is a preferred orientation for Cyt-c on each negatively charged surface. The larger the surface charge density, the closer to –1.0 the cosine of orientation angle is, and the narrower the orientation distribution is. The direction of the dipole of Cyt-c is more anti-parallel to the unit vector normal to the surface and this also indicates that the electrostatic interactions dominate for negatively charged surfaces investigated in this work. The dipole moment of Cyt-c is an important factor to determine the orientation of Cyt-c on negatively charged surfaces. This charge-driven mechanism of protein orientation is consistent with the finding in this group's previous work for the study of antibody orientation by using a residue model.

Figures 3.2(a)-(c) display the final Cyt-c configurations by MD simulations on carboxyl-terminated SAMs with dissociation degrees of 5%(a), 25%(b), and 50%(c). For these negatively charged surfaces, more strongly charged surface forms more salt bridges COO^-/NH_3^+ with Cyt-c and provides stronger electronic coupling with the protein. It is obvious that more side chains of lysine residues direct toward the surface for the SAM with 50% dissociation degree (see **Figure 3.2c**) than for SAMs with 5% or 25% dissociation degrees (see **Figures 3.2a-3.2b**). Du and Saavedra [17] obtained significantly narrower orientation distribution of Cyt-c on sulfonate-terminated SAM than distributions measured previously on other type of SAMs. The experimental observation is consistent with our molecular simulation results, since sulfonate-terminated SAM has a higher surface charge density than carboxyl-terminated SAM.

From **Table 3.1** and **Figures 3.2a-3.2c**, it is found that the heme group is almost perpendicular to the surface. The desired orientation is obtained on carboxyl-terminated negatively charged SAMs. It is long believed that the lysine residues contribute mostly to the final orientation and this cluster of basic residues facilitates their adsorption to acidic surfaces. As mentioned by Fedurco [18], there exist as many as eighteen lysine residues distributed rather homogeneously around the heme on the protein surface. As shown in **Figures 3.2a-3.2c**, the lysine residues (blue) are distributed all over the protein, not only around the heme. With an analysis of negatively charged residue, it was found that all eight glutamic acid residues (red) are far away from the surface. As mentioned by Burkett and Read [19], a few small patches of a large and complicated protein may determine the overall conformation, orientation, and activity of the adsorbed protein. Here, it was found that this part of the glutamic acid residues contributes significantly to the dipole of the protein, and results in the final orientation of the adsorbed Cyt-c as shown in **Figure 3.2**.

Binding sites and electron transport pathway. From the preferred orientation of Cyt-c on carboxyl-terminated SAM with 5% dissociation degree, this study further analyzed the residues close to the surface. They are displayed in **Figure 3.3** with the same orientation as that in **Figure 3.2(a)**. For the lysine residues, LYS25, LYS27, LYS72, and LYS79 are responsible for the strong electrostatic interactions with the surface. This finding clarifies the specific lysine residues that contribute most to the interaction with negatively charged surface. The residues, such as GLN16, THR28, THR47, and ILE81, provide van der Waals interactions with the surface.

The preferred orientation of Cyt-c with respect to the surface shown in **Figure 3.2** would allow for a fast electron transfer. From the simulation-predicted preferred orientation, a possible electron transport pathway is shown in **Figure 3.4**. The redox center consists of heme iron, complexed by four nitrogen atoms of the porphyrin ring, while two amino acids, histidine (HIS18) and methionine (MET80) serve as axial ligands. From **Figure 3.4**, it is clear that the heme edge is very close to the surface. Cyt-c with LYS79 and GLN16 residues directs toward the surface. Thus, the possible ET pathway is iron-HIS18-CYS17-GLN16-surface and iron-MET80-LYS79-surface. Fedurco previously proposed two possible electron transport pathways in his review paper. Simulation results here supported the pathway B of his assumptions.

RMSD and superimposed structures. Root-mean-square deviation (RMSD) is defined as $RMSD = \sqrt{\left\langle \sum_{i=1}^{N} \left(r_a - r_{a,ref} \right)^2 \right\rangle}$. N is the number of all protein atoms. It represents the minimum root-mean-square deviation between one simulated structure and its reference structure. In this work, the crystal structure of Cyt-c was used as the reference structure. The

evolution of RMSD as a function of time for Cyt-c in bulk solution and on SAM surfaces is shown in **Figure 3.5**. The simulated structures of Cyt-c on surfaces and in bulk solution were superimposed on its crystal structure by the molecular graphical program, VMD. They are shown in **Figure 3.6**. This provides a visual assessment of the overall structure of the protein in solution and on surfaces. From **Table 3.1** and **Figure 3.5**, it can be seen that the RMSD value of the bulk solution is 1.60Å, and is comparable with that of tuna Cyt-c in water by Wong et al., i.e., 1.71 Å. From **Figure 3.6(a)**, it can be seen that most features of the secondary structure were preserved for the structure in bulk solution compared with its crystal structure. As found in the work by Stocker et al. [20], the behavior of a protein in solution and in crystal environment is very similar. For the structures of Cyt-c on SAM surfaces with dissociation degree of 5%, 25%, and 50%, the RMSD values are 1.71Å, 1.97Å, and 2.64Å, respectively. They are 6.9%, 23%, and 65% larger than that in bulk solution. Thus, larger conformation change is observed on a charged surface with higher surface charge density. A charged surface with too high surface charge density may cause severe conformation change and denaturation of adsorbed proteins, leading to the loss of its bioactivity. Chen et al. [7] found that no redox peaks were observed for Cyt-c adsorbed on sulfonate SAM. Since SO_3^- terminated SAM is strongly charged, the interactions between the SAM surface and the protein are also strong. However, too strong interactions may cause much larger conformation change of the adsorbed protein, and result in the denaturation of adsorbed Cyt-c. This is possibly why there is no redox peak observed for Cyt-c adsorbed on sulfonate SAM. In **Figure 3.6(b)**, for the 5% case, most of the secondary structure of Cyt-c is retained. This surface could be compared with the hydrophilic surfaces by Tobias et al. and Nordgren et al. [22] since the dissociation degree is not high and electrostatic interactions are not very strong. Tobias et al. found that the secondary structure of the adsorbed Cyt-c, dominated by α-helices, was not significantly affected. Nordgren et al. [22] also found that the overall protein structure was largely conserved, except at each end of the sequence and in one loop region. With the increase of surface charge density, the structure of adsorbed Cyt-c is more distorted, as shown in **Figures 3.6c**-**3.6d**. In terms of RMSD, the structure of the 5% case is closer to that of Cyt-c in bulk solution than that of the 50% case, which shows that the Cyt-c structure on this surface more resembles that of native state and this surface could be used to immobilize Cyt-c for practical applications, since both desired orientation and native conformation are acquired on this surface. In previous studies, Tobias et al. [23] obtained the RMSD values of 3.2Å and 2.9Å for yeast Cyt-c on hydrophobic and hydrophilic surfaces in vacuum, respectively. Due to the screened protein-SAM interactions in water solutions, the RMSD values of fully hydrated Cyt-c are smaller compared with their results. Nordgren et al. [22] observed the dependence of RMSD values on the amount of water molecules and thought that more water molecules helps maintain protein structure in

simulations more akin to its crystal structure.

Radius of gyration and eccentricity. The radius of gyration of a protein, R_G, is defined as $R_G = \sqrt{\frac{1}{M}\sum_{i=1}^{N} m_i r_i^2}$; where M is the molecular weight of the protein; m_i and r_i are the mass and position of each atom, respectively. It represents a mass weighted root-mean-square average distance of all atoms in a protein from its center of mass, which could characterize the overall size of a protein. From **Table 3.1**, it can be seen that the gyration radii of Cyt-c are 12.88Å when solvated in bulk solution, and 12.96Å, 13.03Å, and 13.05Å when adsorbed on SAM surfaces. They are 1.9%, 2.5%, 3.1%, and 3.2% larger than that of its crystal structure, 12.64Å. The gyration radii of Cyt-c on surfaces are 0.62%, 1.16%, and 1.32% larger when compared with that in bulk solution. The gyration radius of Cyt-c solvated in bulk solution, 12.88Å, is almost equal with that in dense solution 12.88Å or in sparse solution 12.89 Å by Nordgren et al. [22]. They also observed increase of gyration radius when adsorbed on surfaces.

The eccentricity of a protein is another parameter that could be used to characterize the overall shape of a protein. It is defined as 1 - I_{ave}/I_{max}, in which I_{max} is the maximal principal moment of inertia and I_{ave} is the average of three principal moments of inertia. From **Table 3.1**, it could be seen that for the 50% case, eccentricity is much smaller than other cases. Since the long axis of the ellipsoidal protein is parallel to the surface and the protein stretches in the direction normal to the surface, Cyt-c looks more globular. While for other cases, the values of eccentricity are close to each other.

Dipole. Dipole is defined as $\vec{\mu} = \sum_{i=1}^{N} q_i (r_i - r_{COM})$, where q_i is the partial charge of each atom, and r_{COM} is the position of the center of mass of the protein. The evolution of dipole moment as a function of time for Cyt-c in bulk solution and on SAM surfaces is displayed on **Figure 3.7**. As shown in **Table 3.1** and **Figure 3.7**, the dipole moments of Cyt-c in bulk solution and on the 5% surface are slightly larger than that in its crystal state. The dipole moment (279D) of Cyt-c in bulk solution is very close to that (271D) of Cyt-c on the 5% dissociated carboxyl-terminated SAM. While the dipole moments of Cyt-c on more strongly charged SAM surfaces with 25% and 50% dissociation degrees are 1.3 and 2.4 times larger than that in bulk solution. The much larger dipole moments are due to the larger structural change induced by more strongly charged surfaces, because of stronger attraction between the positive lysine residues and the negatively charged surface and repulsion between the negative glutamic acid residues and the negatively charged surface. The importance of dipole moment and its change was seldom addressed in previous simulation studies of protein adsorption. The dipole moment of Cyt-c on the 50% surface is much larger

than that of Cyt-c on other surfaces. Although larger dipole and stronger charged surface favor narrower protein orientation distribution, much larger protein conformation change from its native structure on this surface may cause the loss of bioactivity of adsorbed Cyt-c. As pointed out by Fedurco [18], long-range electrostatic forces, acting at the polarized electrochemical interface, can bring this highly charged metalloprotein into the adsorbed state, in which protein unfolding and spin-state changes on the heme iron might occur. From this work and experiments, the conformation change of adsorbed Cyt-c on strongly dissociated negatively charged surface would be too large. Native state conformation cannot be conserved, which is not favorable for practical applications.

Table 3.1 Averaged properties of Cyt-c by MD simulations.

	Orientation	Heme angle	R_{gyr}(Å)	Eccentricity	RMSD(Å)	Dipole(D)
Crystal			12.64	0.144		255
Bulk			12.88	0.143	1.60	279
5%	-0.75	81	12.96	0.151	1.71	271
25%	-0.86	93	13.03	0.145	1.97	364
50%	-0.99	109	13.05	0.138	2.64	661

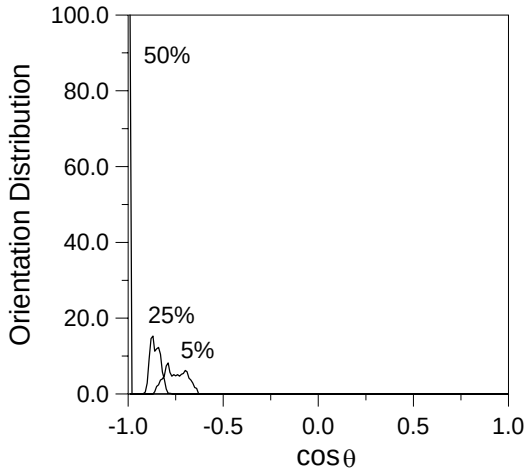

Figure 3.1 Orientation distribution of Cyt-c on carboxyl-terminated SAMs.

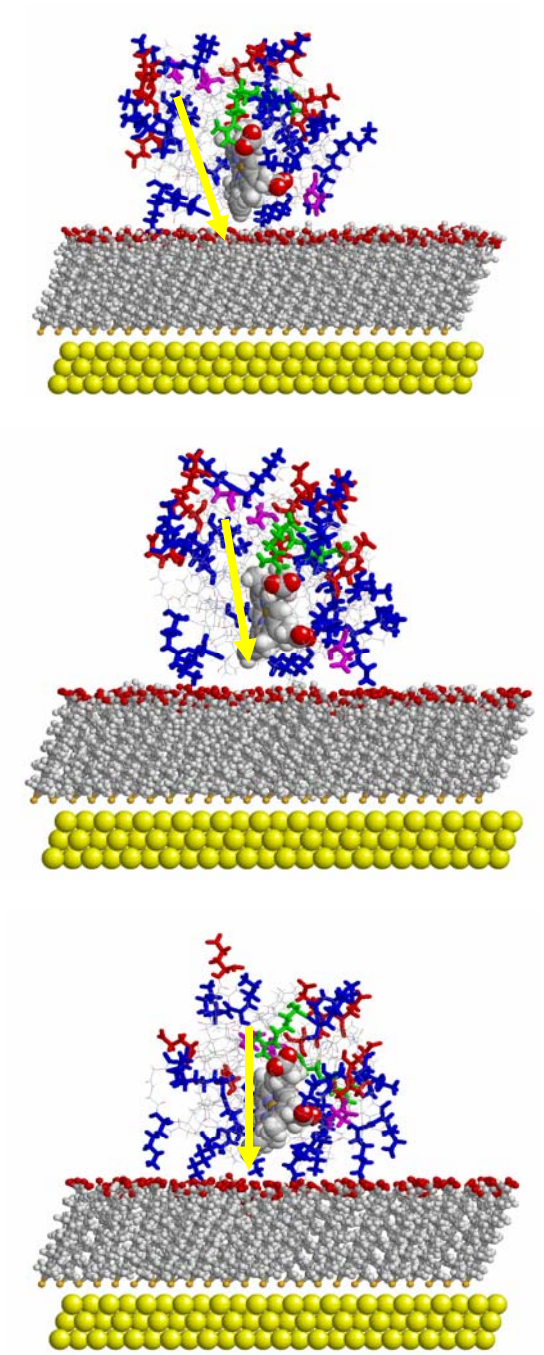

Figure 3.2 Cyt-c configurations on carboxyl-terminated SAMs with dissociation degrees of 5%(a), 25%(b), and 50%(c). For clarity, water molecules and ions are not shown. The yellow space-filled representation is for gold; ball-stick representation for SAM; CPK space-fill representation for heme; stick representation for charged residues, LYS(blue), ARG(green), GLU(red), ASP(magenta); wire-frame representation for other residues in Cyt-c. The yellow arrow indicates the direction of the dipole of Cyt-c.

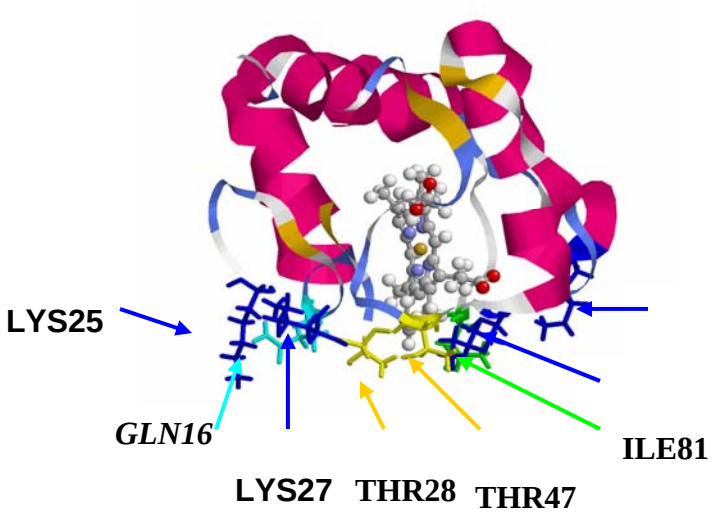

Figure 3.3 Residues of Cyt-c near the SAM surface with 5% dissociation degree.

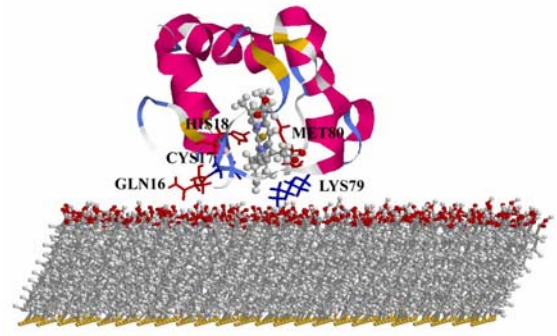

Figure 3.4 Simulation-predicted electron transfer pathway of Cyt-c on negatively charged surfaces.

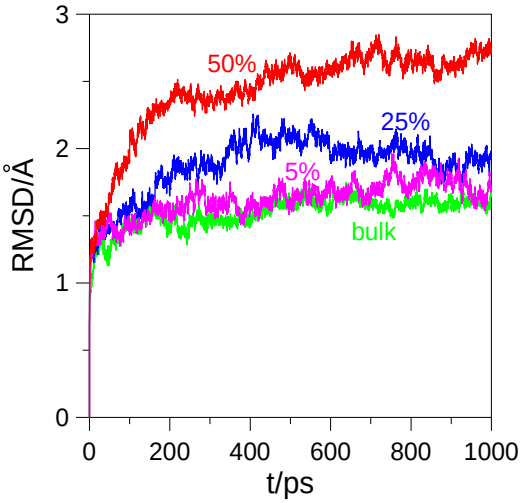

Figure 3.5 RMSD as a function of time for Cyt-c in bulk solution and on SAM surfaces.

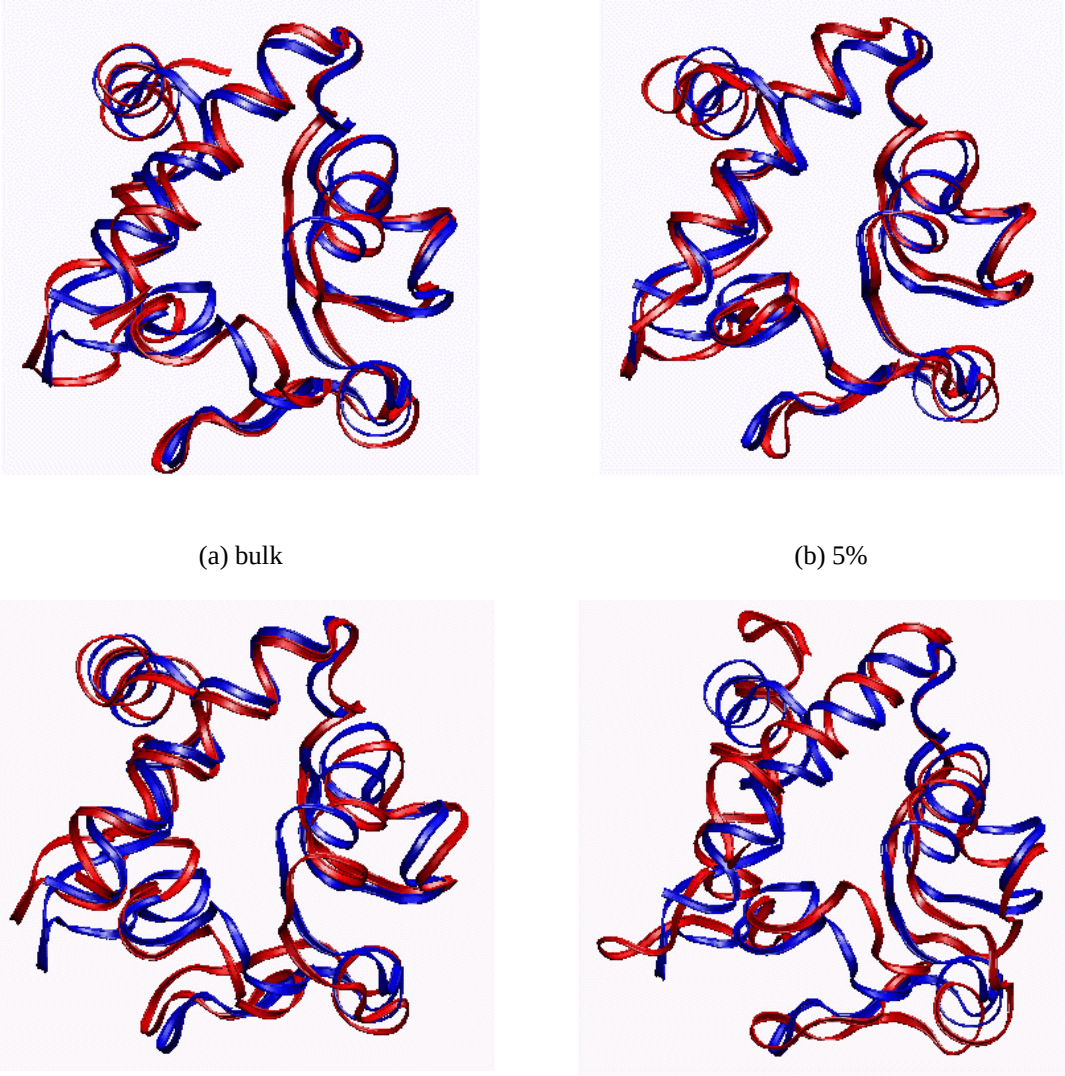

(a) bulk (b) 5%

(c) 25% (d) 50%

Figure 3.6. Simulated structure of Cyt-c (red) in bulk solution (a) and on SAM surfaces with dissociation degrees of 5%(b), 25%(c), 50%(d) superimposed by the crystal structure of Cyt-c (blue).

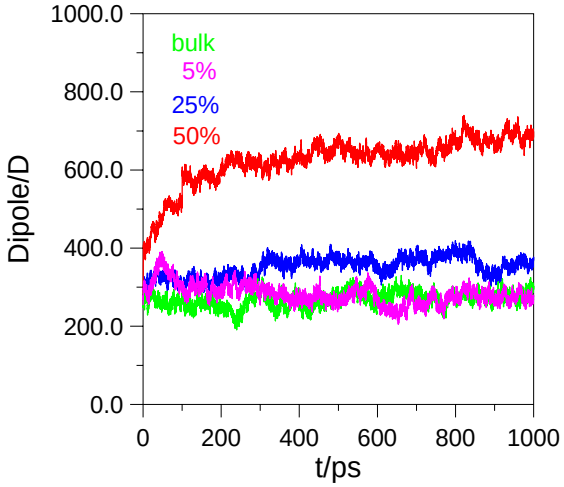

Figure 3.7. Dipole moment as a function of time for Cyt-c in bulk solution and on SAM surfaces.

4. Controlling Protein Orientation on Charged Surfaces

Physical adsorption of antibody: Physical adsorption behavior of the two iso-type IgGs (IgG1 and IgG2a) on two different charged surfaces (COOH and NH_2 terminated SAMs) was investigated. The isoelectric points (IEPs) of IgG1 and its F_{ab} and F_c fragments were measured to be 6.8, 8.3 and 6.0, respectively. The IEPs were determined using isoelectric focusing with PhastGel media, pH range 3-9, and silver staining (PhastSystem, Pharmacia). IgG1 adsorption exhibits a maximum around its IEP (**Figure 4.1**). These results agree with those of Buijs and co-workers [1] on negatively charged silica and hydrophobic polymeric surfaces. The adsorbed amount of both iso-type antibodies on the COOH surface is much higher than that on the NH_2 surface. This trend was also found in the work of Silin *et al*. [21]. However, the total adsorbed amount from this work is about 80% higher than theirs due to the differences in ionic strength and surface charge. Low-quality SAMs formed from $NH_2CH_2CH_2SH$ and relatively high ionic strength (50mM) were used in their work. Compared with the results reported by Buijs and co-workers [1], the adsorbed amount of IgGs on the COOH surface from this work is 20% more than that on negatively charged silica from their experiments. Again, this is caused by the difference in surface charge and

ionic strength. In this work, 2.1 mM PBS along with 0.3mM NaCl was used, while 5mM was used in their experiments. Lower ionic strength is used in this work to maximize electrostatic interactions for the oriented adsorption of IgGs. At lower ionic strength, the average inter-ionic distance is maximized and larger inter-ionic forces will promote the adsorption of IgGs and orientate IgGs by electric field near charged surface. At higher ionic strength, results here showed that less IgGs adsorb on both COOH and NH_2 surfaces. For biosensors, it is desirable to have more immobilized IgGs. Thus, low ionic strength solutions were used in these experiments. In addition, it can be seen from **Figure 4.1** that IgG2a adsorbs more than IgG1 on the lower-coverage NH_2 surface because IgG2a is usually thought to be more flexible than IgG1.

It is interesting that the maximum adsorption of antibody occurs at the same pH value on both positively and negatively charged surfaces. On neutral surfaces, it is expected that the maximum adsorption should occur at the IEP of the protein. For systems where electrostatic interactions play an important role, the maximum adsorption will be affected by charges from both adsorbate and adsorbent and will be shifted away from the IEP. For globular shape molecules, it is expected that the maximum adsorption will shift to lower pH from its IEP on the negatively charged COOH surface while to higher pH from its IEP on the positively charged NH_2 surface when surface charge densities do not vary much over the pH range studied as in this work. Results in this study show that the maximum adsorption on the COOH surface indeed shifts to lower the pH value as expected. However, the maximum adsorption on NH_2 surfaces also shifts to the lower pH value. This behavior may be due to the asymmetric structure of IgG along the direction from F_c to F_{ab}.

The orientation of an antibody can be judged from the adsorbed amount. A simple relationship between adsorbed amount and molecular configuration on surfaces was given by Buijs and co-workers [1]. Based on their calculations, for all "end-on" (F_c closer to surface) and "head-on" (F_{ab} closer to surface) orientations, surface coverage should be between 2.6 and 5.5 mg/m^2, depending on the angle between two F_{ab} fragments. For the "side-on" (F_c and one of F_{ab}s closer to surface while another F_{ab} away from surface) orientation, surface coverage should be near 2.0 mg/m^2. It is expected that true IgG coverage will be lower than

the values for these highly idealized packing structures if one takes into account steric effects. From **Figure 4.1**, it can be seen that the adsorbed amount of ~5 mg/m^2 is achieved on the COOH surface near the IEP. Thus, IgG1 on the COOH surface could be thought to have "head-on" (not "end-on" as discussed later) orientation as described by Buijs and co-workers. However, lower surface coverage suggests that IgG1 on the NH_2 surface might have orientations ranging between "end-on" and "side-on". This analysis is based on a monolayer model. All surfaces with adsorbed antibody were studied by AFM. Results show that there is no obvious multilayer formed.

HCG to anti-hCG ratio: The hCG to adsorbed anti-hCG ratio is a more important criterion for antibody orientation. Higher ratio indicates that more F_{ab} fragments are accessible. The minimum antigen response was found near pH 5.8 for IgG1 on the COOH surface (**Figure 4.1**). In contrast, near pH 6.6, there is a maximum hCG response to adsorbed IgG1 on the NH_2 surface (**Figure 4.1**). The hCG/anti-hCG (IgG1) ratio in **Figure 4.2** shows large difference between on NH_2 and COOH surfaces. Higher hCG/anti-hCG (IgG1) ratios and the occurrence of a maximum near its IEP indicate that more F_{ab} fragments are accessible on the positively charged NH_2 surface than on the negatively charged COOH surface. At the maximum, an hCG/anti-hCG ratio of 0.48 was observed when 1μg/ml hCG was used in this work (**Figure 4.2**). If a hCG concentration of 10μg/ml or higher (saturated concentration) was used, a hCG/anti-hCG ratio as high as 0.8 was observed. On the negatively charged surface, lower hCG/anti-hCG ratios and the occurrence of a minimum near its IEP indicate that less F_{ab} fragments are accessible. When the pH is far away from IEP, the hCG/anti-hCG ratios become higher on the COOH surface and lower on the NH_2 surface.

In addition, antibody behavior on CH_3 terminated SAMs was also studied. CH_3 terminated SAMs are used to represent a neutral (hydrophobic) surface. **Figure 4.3** shows hCG/anti-hCG (IgG1) ratio as a function of NH_2 ratio in NH_2/CH_3 mixed SAMs. When the percentage of NH_2 in the mixed SAMs decreases, the surface charge density deceases. Thus, the hCG/anti-hCG ratio also decreases. As shown in **Figure 4.3** together with previous results (**Figure 4.2**) on the negatively charged COOH surface, it can be seen that the

hCG/anti-hCG ratio increases from negative to neutral to positive surfaces at pH 6.2. This demonstrates how surface charge affects antibody orientation. The adsorbed amounts of IgG1 on negative, neutral, positive surfaces are 5, 2.2, 2.4 mg/m^2, respectively.

Considering both adsorbed amount and hCG/anti-hCG ratio from SPR experiments, it is believed that IgG1 mainly has "head-on" orientation on the COOH surface, orientations ranging between "end-on" and "side-on" on the NH_2 surface, and "lying" (F_c and two F_{ab}s closer to surface) orientation on the CH_3 surface as illustrated in **Figure 4.4**. Surface charge and IgG1 dipole moment are mainly responsible for such distinct orientations on different surfaces. Antibodies have a Y shape structure with two F_{ab} fragments and one F_c fragments. From a geometrical point of view, two F_{ab} fragments on the surface ("head-on" orientation) is more stable than a single F_c fragment on the surface ("end-one" orientation). A strong dipole moment could help stabilize antibody orientation on surfaces. Furthermore, previous work by Buijs et al. [1] shows that F_{ab} is more easily denatured than F_c, which makes two F_{ab} fragments on the surface ("head-on" orientation) even more stable. This is why IgG1 has a stable "head-on" orientation on the COOH surface while orientations ranging between "end-on" and "side-on" on the NH_2 surface. This is also why IgG1 adsorbs more on COOH than NH_2 surfaces. From the biosensor application point of view, a positively charged NH_2 surface is a better candidate for monolayer-based biosensors with higher antigen response, 55% higher than conventional methods based on CH_3 surface. For the negatively charged COOH surface, the best way to get better orientation is to immobilize IgG under pH away from its IEP and/or at relatively high salt concentrations.

It should be pointed out that steric effects and antibody activity do not affect the hCG/anti-hCG ratio significantly. Instead, antibody orientation mainly determines the hCG/anti-hCG ratio. Recent experiments by this group show that the adsorbed amount of acid-pretreated IgG1 on CH_3 terminated SAMs (~5mg/m^2) is as high as that of native IgG1 on COOH terminated SAMs. Antigen response to the adsorbed acid-pretreated IgG1 layer is comparable to that of native IgG1 on NH_2 terminated SAMs. This indicates that lower antigen response to the adsorbed native IgG1 is due to undesired antibody orientation instead of steric effects. In this work, the same cross-linking conditions were used to immobilize the

antibodies on COOH and NH_2 surfaces. Thus, it is expected that the effect of cross-linking on antibody bioactivity will be similar. Furthermore, the antibody layer is thicker on COOH than NH_2 SAMs. If antibody has the "end-on" orientation on the COOH surface (i.e., F_{ab} containing immunoreaction sites is away from the surface), it should be less denatured by the surface and have better activity. However, this is not the case. Thus, surface effects on antibody bioactivity should be larger on NH_2 SAMs with a thinner protein film (~8nm) than COOH SAMs with a thicker protein layer (~15nm) if any. Therefore, the variations in the hCG/anti-hCG ratio are attributed mainly to the differences in adsorbed protein orientation rather than steric effects or decreases in antibody bioactivity due to crossing-linking or surface effects.

For IgG2a, the hCG response to adsorbed antibody is similar on both COOH and NH_2 surfaces. According to molecular structures from the protein data bank, IgG1 has a "Y" shaped structure while IgG2a has a "T" shape. The dipole moment of IgG1 is two times larger than that of IgG2a based on our simulations. Thus, IgG1 displays distinct orientations on the COOH and NH_2 surfaces. However, IgG2a has many orientations on both charged surfaces due to smaller dipole moment[41]. Furthermore, IgG2a has a more flexible structure and both Fab and Fc fragments are easily adsorbed on the surface. Thus, it is harder to control the orientation of IgG2a using electrostatic forces alone.

AFM results: AFM images of IgG1 on COOH and NH_2 SAMs on single-crystal Au(111) are shown in **Figure 4.5**, which support our previous discussions. First, all images are quite flat without any obvious aggregation. This excludes the possibility that the lower hCG/anti-hCG ratio observed on the COOH surface was caused by limited accessibility to the binding sites due to aggregation. Second, surface roughness increases on the COOH surface. The section analysis in **Figure 4.4** shows a larger height difference on the COOH surface than on the NH_2 surface. This provides more evidence of a "head-on" orientation on the COOH surface. On the COOH surface, there exist some "side-on" orientations, yet most of the antibody molecules have "head-on" orientations. Antibodies with "head-on" orientation are higher than that those with "side-on" orientations, leading to an increase in surface roughness. On the NH_2 surface, most antibody molecules have orientations ranging

between “end-on” and “side-on.” This difference in height should be smaller on NH_2 than on COOH surfaces, leading to smoother surfaces on the NH_2 surface. In fact, due to AFM tip convolution, higher features look larger. Thus, the features on the COOH surface look slightly larger than those on the NH_2 surface.

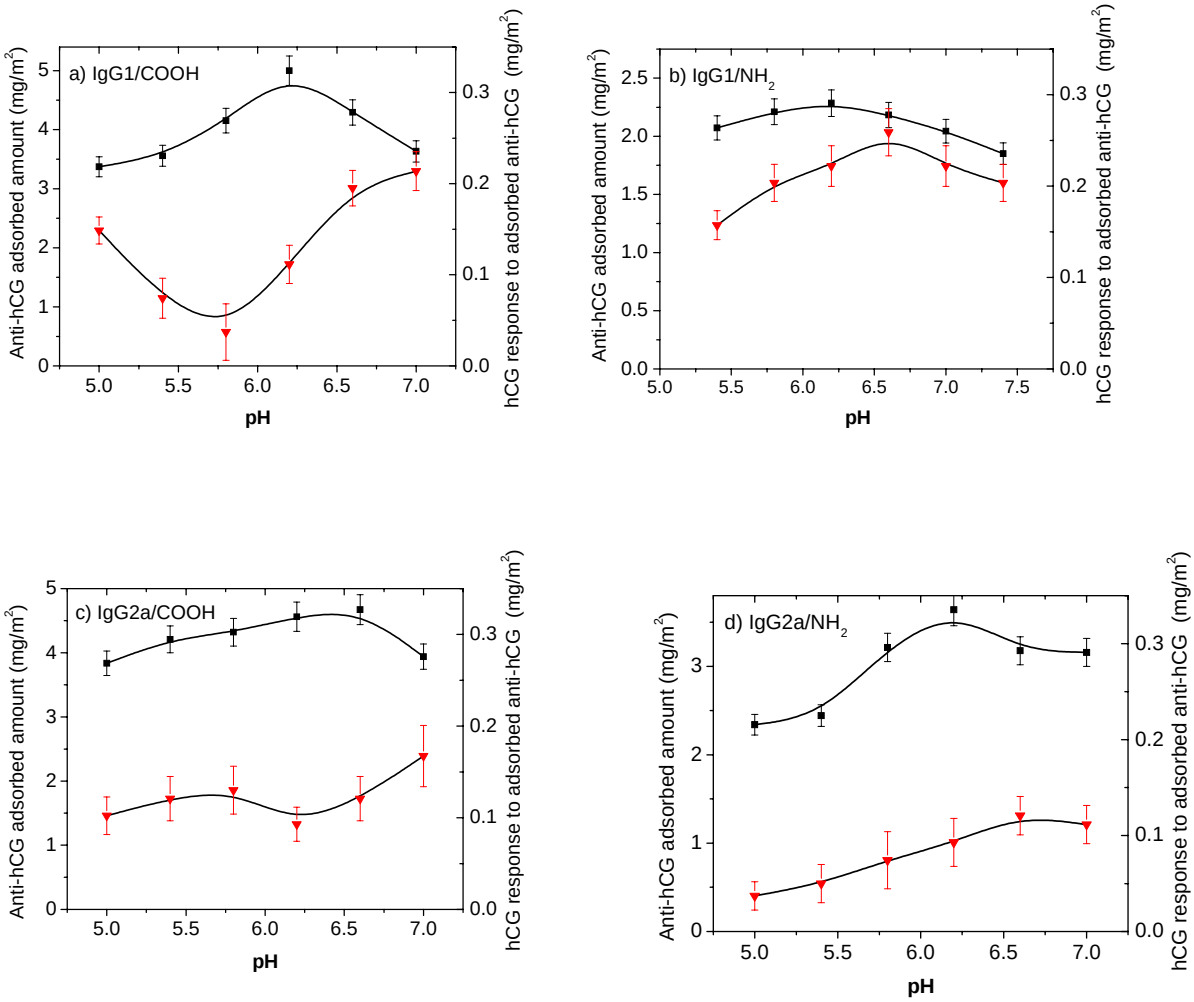

Figure 4.1 Plateau antibody adsorption (-!-) from 13 µg/ml as a function of pH for monoclonal IgG1 and IgG2a on COOH and NH2 terminated SAMs and corresponding immunoreaction from 1µg/ml hCG solution (-B-). a) IgG1 on the COOH surface, b) IgG1 on the NH_2 surface, c) IgG 2a on the COOH surface, and d) IgG2a on the NH_2 surface.

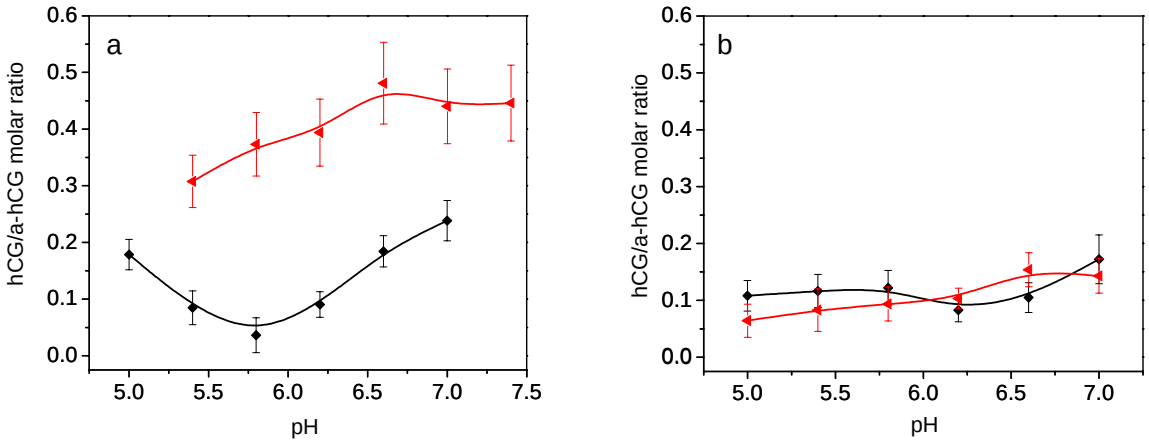

Figure 4.2 hCG/anti-hCG (IgG1 or IgG2a) molar ratios on COOH or NH_2 surfaces as a function of pH. a) IgG1 on the COOH surface (-Λ-) and on the NH_2 surface (-Ω-); b) IgG 2a on the COOH surface (-Λ-), and on the NH_2 surface (-Ω-).

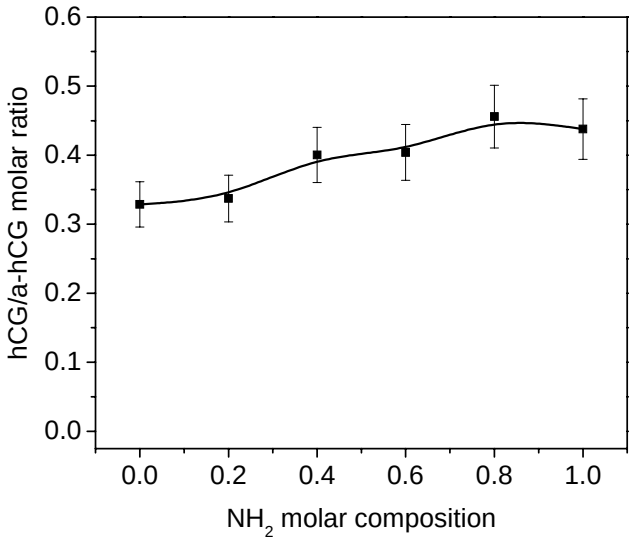

Figure 4.3 hCG/anti-hCG molar ratio of IgG1 as a function of NH_2 molar composition in mixed NH_2/CH_3 SAMs. The hCG/anti-hCG ratio increases as NH_2 surface composition increases.

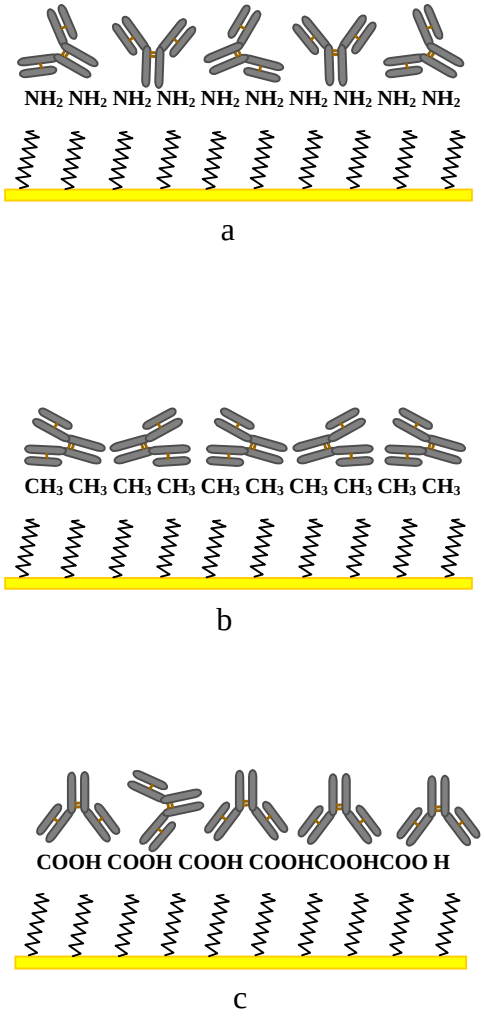

Figure 4.4 Illustration of IgG1 orientations on COOH, NH_2, and CH_3 surfaces.

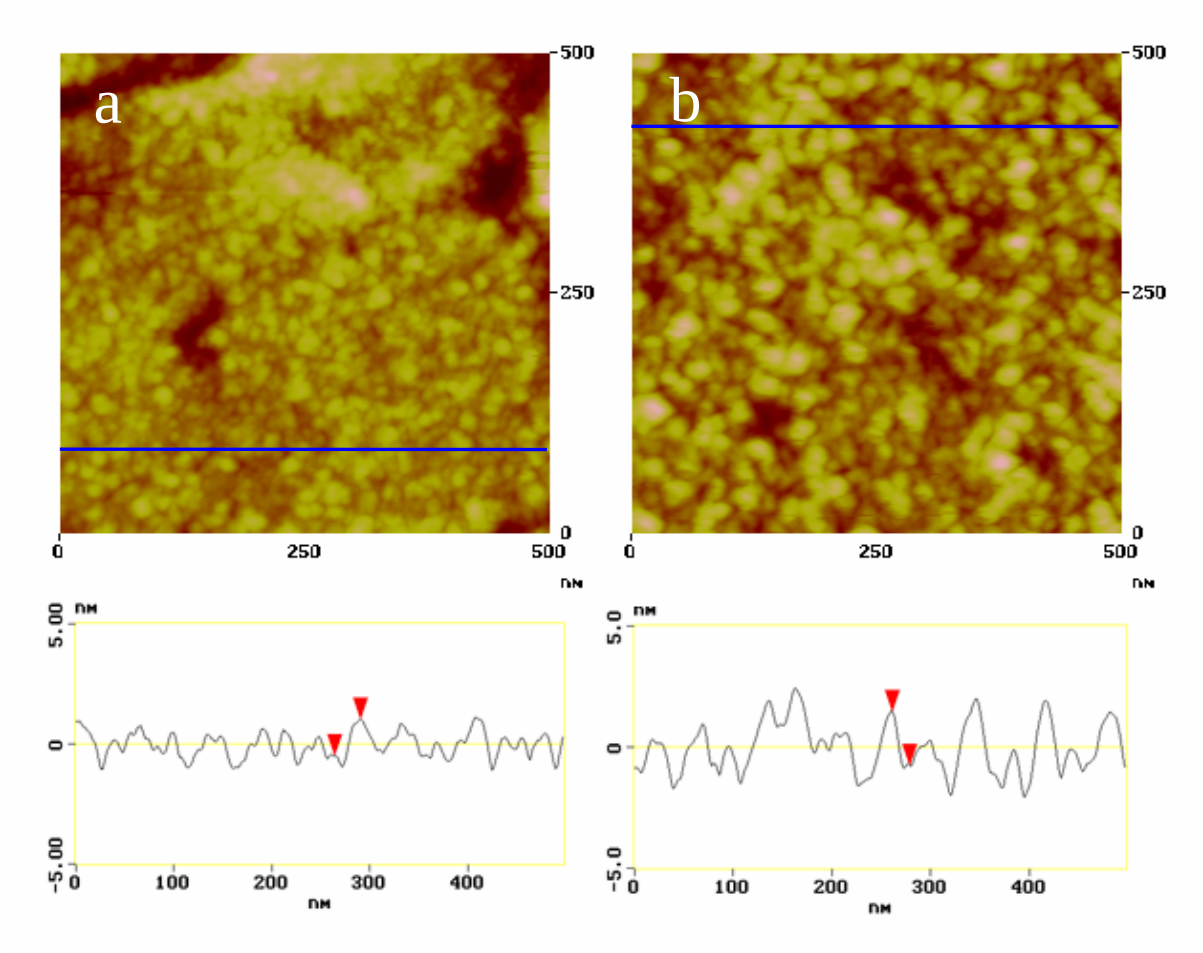

Figure 4.5 AFM images and corresponding cross sections of IgG1 on (a) NH_2 and (b) COOH surfaces.

5. Probing Protein Orientation on Charged Surfaces

Recently, Chen *et al* [24] showed that the orientation of adsorbed anti-hCG can be controlled by appropriately tuning the microenvironments of the adsorption process (i.e., surface and solution properties). The IEP of anti-hCG (pH 6.8) lies between those of its $F(ab')_2$ (pH 8.5) and F_c (pH 6.1) fragments. At the IEP of anti-hCG, although the net charge of the whole molecule is zero, its $F(ab')_2$ part is positively charged while its F_c part is negatively charged. That is, there is a dipole pointing from its F_c to its $F(ab')_2$ fragments. It was predicted from recent molecular simulation studies that anti-hCG will have a "head-on" orientation ($F(ab')_2$ is closer to the substrate) on a negatively charged substrate while "end-on" orientation (F_c is closer to the substrate) on a positively charged substrate. The SPR biosensor was used to determine antigen/antibody immuno-reaction on carboxyl (negatively charged) and amino (positively charged) terminated SAMs. The hCG/anti-hCG ratio would be zero and two for perfect "head-on" and "end-on" orientations, respectively. It was found that on the negatively charged carboxyl terminated SAMs, the hCG/anti-hCG ratio is around 0.1 at the IEP of anti-hCG, indicating that most of anti-hCGs have a "head-on" orientation. On the positively charged amino terminated SAMs, the hCG/anti-hCG ratio could be as high as 0.8 at the IEP of anti-hCG, indicating that anti-hCGs may have mixed orientations ranging between "end-on" and "side-on" as illustrated in **Figure 5.1**. The orientation of anti-hCG on positively charged amino terminated SAMs is not totally "end-on". This could be due to the fact that the surface charge of amino terminated SAMs is not high enough. In this work, carboxyl and amino terminated SAMs will be used for ToF-SIMS studies since SPR experiments indicate that different orientations of absorbed antibodies are expected on these two controlled surfaces. However, by physical adsorption, the adherence between the anti-hCG molecules and the surface is relatively weak, the adsorbed anti-hCG molecules still have chance to rotate or move on the surface during the process of rinsing with DI water and under the ultra-high vacuum environment of static ToF-SIMS analysis. Thus, chemical linkers such as NHS/EDC and glutaraldehyde were applied to carboxyl and amino terminated SAMs, respectively **(Figure 5.2)**. The orientation/conformation of chemically linked anti-hCG on surfaces can be better preserved. It should be pointed out that instead of using pure COOH- terminated SAMs, this study used a mixture of $HS(CH_2)_{15}COOH$ and $HS(CH_2)_{11}OH$ (0.05: 0.95 in solution) to improve the efficiency of the reaction between the COOH surface group and NHS/EDC by minimizing any possible steric effects (i.e., the size of the NHS group). A detailed characterization of both the unmodified and modified SAMs was performed to understand their chemistries and surface charge.

Characterization of the unmodified and modified SAMs. Table 5.1a presents the atomic percentages of the mixed COOH- and OH- terminated and NH_2- terminated SAMs

from XPS before and after modification by their respective cross-linkers. **Table 5.1b** lists theoretical values for the elemental compositions of the four types of thiol molecules expected to be present in either unmodified or modified SAMs, i.e., $HS(CH_2)_{11}OH$, $HS(CH_2)_{15}COOH$, $HS(CH_2)_{15}COONC_4H_4O_2$ (the product of $HS(CH_2)_{15}COOH$ modified by NHS/EDC), and $HS(CH_2)_{11}NH_2$. However, no simple thiol molecule can be used to represent the product of $HS(CH_2)_{11}NH_2$ SAMs modified by glutaraldehyde, in which glutaraldehyde polymerizes first and forms a network over the $HS(CH_2)_{11}NH_2$ SAMs **(Figure 5.2).** It can be seen that for mixed COOH- and OH- terminated SAMs modified by NHS/EDC, a decrease in carbon and an increase in oxygen were seen as compared with unmodified counterparts, while nitrogen, characteristic of NHS, was only detected in the spectra of the modified samples. These changes are consistent with theoretical calculations. From $HS(CH_2)_{15}COOH$ to $HS(CH_2)_{15}COONC_4H_4O_2$, the atomic composition of carbon decreases from 84.2% to 76.9%, while oxygen increases from 10.5% to 15.4%. For NH_2-terminated SAMs modified by glutaraldehyde, increases in carbon and oxygen were seen as compared with their unmodified counterparts, while a decrease in nitrogen can be seen. Although theoretical values for the elemental compositions of the modified $HS(CH_2)_{11}NH_2$ SAMs are not available, these changes measured by XPS are reasonable because glutaraldehyde consists of carbon and oxygen, while nitrogen is only present in $HS(CH_2)_{11}NH_2$. In general, consistency between the measured atomic percentages and the stoichiometric elemental compositions for both the unmodified and modified samples suggests satisfactory SAM formation and successful modification. However, as compared with the stoichiometric compositions, oxygen peaks were seen in both unmodified and modified NH_2- terminated SAMs, which could be due to the oxidation of the $HS(CH_2)_{11}NH_2$ thiols, as found in our other studies. For SAMs, the atomic composition of sulfur is lower than its theoretical value due to attenuation of sulfur photoelectrons away from the surface.

Both positive and negative ToF-SIMS spectra were obtained for unmodified and modified carboxyl and amino terminated SAMs. **Table 5.2** lists the relative intensities of some characteristic peaks and the molecular ions of the three thiol molecules present in either unmodified or modified mixed COOH- and OH- terminated SAMs normalized to their total ToF-SIMS spectral intensities. A decrease in the relative intensities of the molecular ions of $HS(CH_2)_{15}COOH$ and an increase in the relative intensities of the molecular ions of $HS(CH_2)_{15}COONC_4H_4O_2$ can be seen after NHS/EDC modification as expected. The molecular ions of $HS(CH_2)_{11}OH$ also show a decrease in their relative intensities, which could be due to their decreased ion yields induced by the introduction of the bulky NHS head groups. Two peaks originating from the NHS group, $C_4H_4NO_2^+$ (m/z=98) and $C_4H_4NO_3^-$ (m/z=114), are detected as strong peaks in the spectra of the modified sample, but only

weakly in the unmodified one, while the OH^- (m/z=17) peak from both carboxyl and hydroxyl groups shows an obvious decrease in the spectra of the modified samples. Similarly, for the NH_2- terminated SAMs, the molecular ions of $HS(CH_2)_{11}NH_2$ decrease after glutaraldehyde modification, and the fragments of $HS(CH_2)_{11}NH_2$ such as NH_4^+ (m/z=18) and CH_4N^+ (m/z=30) also decrease in the spectra of the modified samples as shown in **Tables 5.3**. All of the above differences between the ToF-SIMS spectra of modified and unmodified samples indicate the occurrence of the reactions between the original functional groups (COOH- and NH_2-) and the cross-linkers (NHS/EDC and glutaraldehyde).

In this work, surface charge is an important factor for the orientation of adsorbed anti-hCG. Since chemical linkers were applied to modify the NH_2- and mixed COOH- and OH-terminated SAMs, the surface charge of both unmodified and modified SAMs were measured by AFM in buffer solution to ensure that there exists appropriate surface charge to modulate the orientation of adsorbed proteins after modification by the chemical linkers. A detailed description of how these AFM measurements are performed is given elsewhere [25]. In short, the silicon nitride tip used in our study has a layer of oxide on its surface and bears a negative charge. Thus, in PBS buffer at pH 6.8 and low ionic strength, a repulsive electrostatic force is expected when the tip is approaching a negative surface. Conversely, the tip should be attracted when it gets closer to a positive surface. **Figure 5.3** shows the force between the tip and the sample versus distance curves measured on both modified and unmodified SAMs. A repulsive mode can be seen on both modified and unmodified mixed COOH- and OH- SAMs, while a slightly attractive mode can be seen on both modified and unmodified NH_2- SAMs. Results suggest that after chemical modification by cross-linkers, some surface charge remains. This is consistent with the fact that some unreacted $HS(CH_2)_{15}COOH$ and $HS(CH_2)_{11}NH_2$ thiols are detected from ToF-SIMS analysis after modification (**Tables 5.2 and 5.3**). Furthermore, the dissociation of carboxyl groups and the protonation of amino groups improve when the densities of these surface groups decrease. In addition, NHS head groups on modified COOH terminated SAMs have a tendency to hydrolyze in the aqueous buffer environment, which is another reason for similar surface charge before and after modification of the mixed COOH- and OH- SAMs. For convenience, the mixed COOH- and OH- terminated SAMs will be referred as carboxyl terminated SAMs in the subsequent text.

AFM characterization of protein films. Before ToF-SIMS analysis, AFM was used to characterize all the protein films studied. Some results are shown in **Figure 5.4**. It can be seen that a smooth protein monolayer was formed on all surfaces. This study found that a full coverage of protein is important for the successful detection of protein orientations by ToF-SIMS.

Detection of IgG orientation on different substrates. A scores plot (PC1 vs. PC2) of positive ion ToF-SIMS spectra for anti-hCG adsorbed onto amino and carboxyl terminated SAMs as well as its $F(ab')_2$ and F_c fragments adsorbed onto Au(111) is shown in **Figure 5.5**. The PCA model was developed using the first two PCs from PCA of the positive ion spectra of $F(ab')_2$ and F_c adsorbed onto Au(111). ToF-SIMS spectra of all adsorbed protein films were then projected onto this model. The first PC captures 94.1% of total variance in the data set and clearly distinguishes different groups. By examining the scores of protein spectra on PC1, it can be seen that anti-hCG behavior on these carboxyl and amino terminated SAMs are clearly differentiated by PCA. The ToF-SIMS spectra for anti-hCG adsorbed on amino terminated SAMs with mixed "end-on" and "side-on" orientations are more similar to those for $F(ab')_2$ while the ToF-SIMS spectra for anti-hCG adsorbed on carboxyl terminated SAMs with a "head-on" orientation are more similar to those for F_c. This is consistent with previous SPR experimental results and molecular simulation predictions. Since static ToF-SIMS samples only the outermost 1-1.5 nm region of the adsorbed protein films, it will sample primarily the F_c portion of anti-hCG with a "head-on" orientation and primarily the $F(ab')_2$ portion of anti-hCG with an "end-on" orientation.

Figure 5.6 is similar to **Figure 5.5**, except that the ToF-SIMS spectra for anti-hCG adsorbed on the Au(111) surface were also projected onto the PCA model. It can be seen that this cluster spreads over a large area, overlapping with both groups of anti-hCG adsorbed onto carboxyl and amino terminated SAMs. This is partly due to the random orientation of anti-hCG on Au(111). It also can be seen that the within-group scattering of the F_c is higher than the other groups. This could be due to the random orientation of F_c on the Au(111) surface and the purity of the F_c fragment sample used in our study. On the F_c fragment lane, there are two light bands in addition to the major 25kDa band, indicating the presence of impurity in the F_c fragment sample. Also the 25kDa band is broader in the F_c sample.

Furthermore, it was found that the PCA scores of ToF-SIMS spectra for adsorbed protein films are sensitive to protein surface concentration (data not shown). This could be due to the more extensive conformation changes expected to occur for low-coverage protein films in the ultra-high vacuum environment needed for static ToF-SIMS measurements. In addition, higher background interference from the chemical linkers is expected for samples with low protein coverage, which is discussed in the next paragraph.

To ensure that all adsorbed protein films in this study undergo roughly the same extent of conformational change during ToF-SIMS analysis and to minimize the magnitude of this conformation change, high protein surface concentrations were used for all the samples studied. Both AFM images (**Figure 5.4**) and the ratios of the ToF-SIMS total protein peak intensity to the total spectral intensity obtained from ToF-SIMS spectra were used to monitor

surface coverage. In this work, only those spectra with the total protein peak intensity greater than 33% of the total spectral intensity were used.

Since protein films examined in this work are immobilized onto three different types of substrates, [i.e., amino terminated SAMs, carboxyl terminated SAMs, and bare Au(111)], the influence of the substrate on the secondary ion yield (i.e., the matrix effect) may vary among the samples. However, it is believed that the matrix effect on the differences among different groups of ToF-SIMS spectra shown in **Figures 5.5 and 5.6** should be negligible. In addition to Au(111), $F(ab')_2$ and F_c were also adsorbed onto amino terminated SAMs as references. The PCA model for **Figure 5.7** was developed using the first two PCs from PCA of the positive ion spectra of $F(ab')_2$ and Fc adsorbed onto amino terminated SAMs, which capture 97.5% of the total variance. ToF-SIMS spectra of all adsorbed protein films were then projected onto this model, as was done for **Figure 5.6**. It can be seen that **Figure 5.7** has a similar organization as **Figure 5.6**, although different references were used. This indicates that matrix effects do not affect the relative relationship among different samples studied in this work.

Besides the matrix effect, another potential interference may come from the background of chemical linkers on SAMs, which may have ToF-SIMS peaks at the same mass as the amino acid peaks. The modified carboxyl and amino terminated SAMs indeed generate some peaks which overlap with those of amino acids from the protein films in ToF-SIMS spectra. However, these results indicate that once covered with a protein monolayer, SAMs with chemical linkers generate little interference, as expected. The sampling depth of ToF-SIMS is only 1-1.5 nm, which is much less than the thickness of the protein monolayer (4-10 nm). Thus, the interference from the background is negligible in this study.

Relating ToF-SIMS spectra to protein structure. In **Figure 5.8**, the loadings plot for PC1 in **Figures 5.5** and **5.6**, reveals the differences in the amino acid compositions of the outer surface of the adsorbed protein films. For peaks loading positively on PC1, such as $C_3H_6N^+$, $C_4H_6N^+$, and $C_8H_{10}N^+$, their intensities contribute to positive PC1 scores. Thus, the relative concentrations of the amino acids corresponding to these peaks, such as lysine, proline and phenylalanine, should be higher in samples with positive PC1. This means that these amino acids should be more prevalent in the F_c fragment, which scores positively on PC1. Conversely, for peaks loading negatively on PC1 their corresponding amino acids should be more prevalent in the $F(ab')_2$ fragment, which scores negatively on PC1. Peaks such as $C_4H_8N^+$, which are not unique to only one amino acid, are more complicated and cannot be used to track a specific amino acid.

The molecular structures of the $F(ab')_2$ and F_c portions of mouse monoclonal anti-hCG are available from the Protein Data Bank [26]. Therefore, the compositions of the twenty

amino acids in these two fragments were obtained and listed in **Table 5.4**. The relative concentration of the amino acids obtained from the protein structure correlates well with those determined by ToF-SIMS, as shown in **Table 5.5**. ToF-SIMS peaks more prevalent in $F(ab')_2$ should have a relative $F(ab')_2/F_c$ composition ratio greater than unity, while peaks more prevalent in F_c indicated by ToF-SIMS results should have a ratio less than unity. It can be seen from **Table 6** that the relative intensities for most of the ToF-SIMS peaks are consistent with the known composition of the anti-hCG.

Tracking anti-hCG orientation by the intensity ratio of certain peaks. Anti-hCG orientation on different substrates could also be tracked by ratioing the intensities of ToF-SIMS peaks from amino acids more prevalent in one fragment than in the other. A similar method was reported previously to track the relative concentrations of proteins in a binary adsorbed protein film [27]. From **Tables 5.4** and **5.5**, it can be seen that serine and tyrosine are more prevalent in $F(ab')_2$, while lysine and phenylalanine are more prevalent in F_c. For the "end-on" orientation (F_c near the surface and $F(ab')_2$ away from the surface), a lower ratio of the intensities of the 56.05 m/z peak (lysine) to the 60.05 m/z peak (serine) and a higher ratio of the intensities of the 107.05 m/z peak (tyrosine) to the 120.08 m/z peak (phenylalanine) are expected. **Figure 5.9** shows these two ratios for $F(ab')_2$, F_c, and anti-hCG on carboxyl and amino terminated SAMs. It can be seen that they follow the expected trend, indicating that anti-hCG orientation can also be tracked by using the ratios of certain characteristic peaks. A T-test for these results shows that the means of the ratios for each sample are significantly different from each other at the 0.05 confidence level, except for the 56/60 ratio of F_c on Au(111) and anti-hCG on carboxyl terminated SAMs ($p = 0.07$). However, although this method is relatively simple, it is not as comprehensive as the combined ToF-SIMS and PCA method.

Table 5.1a XPS atomic percentage (%) of the unmodified and modified NH_2- and mixed COOH- and OH- SAMs. The signal from the gold substrate is not included in the XPS compositions so that the measured compositions can be compared directly to the stoichiometric compositions.

	mixed $C_{15}COOH$ and $C_{11}OH$	mixed $C_{15}COOH$ and $C_{11}OH$ modified by NHS/EDC	$C_{11}NH_2$	$C_{11}NH_2$ modified by glutaraldehyde
C	84.5	82.1	79.4	80.0
O	12.4	13.1	8.0	14.7
S	3.0	3.1	3.7	1.3
N	0	1.6	8.9	4.0

Table 5.1b Stoichiometric compositions (%) of some pure alkanethiols.

	$C_{11}OH$	$C_{15}COOH$	$HS(CH_2)_{15}COONC_4H_4O_2$	$C_{11}NH_2$
C	84.6	84.2	76.9	84.6
O	7.7	10.5	15.4	0
S	7.7	5.3	3.9	7.7
N	0	0	3.9	7.7

Table 5.2 ToF-SIMS relative intensities of some characteristic peaks and the molecular ions of $HS(CH2)_{11}OH$, $HS(CH_2)_{15}COOH$, and $HS(CH_2)_{15}COONC_4H_4O_2$ in the unmodified and modified mixed COOH- and OH- SAMs normalized to their total spectra intensities*.

samples / peaks	mixed $C_{15}COOH$ and $C_{11}OH$	mixed $C_{15}COOH$ and $C_{11}OH$ modified by NHS/EDC	Ratio (modified/ unmodified)
Molecular Ions			
$HS(CH_2)_{11}OH$			
[M-H]	3.4E-4(1.1E-5)	1.2E-4(1.9E-5)	0.35
[M-H+3O]	4.6E-2(2.4E-3)	1.7E-3(1.7E-4)	0.036
Au_2[M-H]	9.0E-4(3.4E-5)	4.9E-4(4.3E-6)	0.54
Au$[M-H]_2$	3.8E-4(4.7E-5)	2.1E-4(3.8E-6)	0.55
AuM	5.0E-4(8.1E-5)	2.9E-4(8.5E-6)	0.58
$HS(CH_2)_{15}COOH$			
[M-H]	3.9E-4(7.0E-6)	1.1E-4(2.5E-5)	0.28
[M-H+3O]	3.0E-2(2.3E-3)	2.3E-4(3.6E-5)	0.008
Au_2[M-H]	1.3E-4(9.4E-5)	1.0E-5(2.4E-6)	0.08
Au$[M-H]_2$	0	0	0
AuM	5.1E-5(4.3E-6)	7.2E-6(4.0E-6)	0.14
$HS(CH_2)_{15}COONC_4H_4O_2$			
[M-H]	0	0	
[M-H+3O]	0	2.7E-4(1.6E-5)	
Au_2[M-H]	0	5.3E-5(4.9E-6)	
Au$[M-H]_2$	0	0	
AUM	0	4.1E-5(5.8E-6)	
Characteristic Peaks			
$C_4H_4NO_2^+$	7.3E-5(2.4E-6)	1.9E-3(8.3E-5)	26
$C_4H_4NO_3^-$	1.2E-4(5.6E-6)	2.8E-2(6.0E-4)	233

* Three samples were measured for each SAM. Data shown are the average results with standard deviation (in brackets).

Table 5.3 ToF-SIMS relative intensities of some characteristic peaks and the molecular ions of $HS(CH_2)_{11}NH_2$ in the unmodified and modified $C_{11}NH_2$ SAMs normalized to their total spectra intensities*.

peaks \ samples	$C_{11}NH_2$	$C_{11}NH_2$ modified by glutaraldehyde	Ratio (modified/ unmodified)
Molecular Ions			
$HS(CH_2)_{11}NH_2$			
[M-H]	8.2E-5(4.0E-6)	1.4E-5(2.2E-6)	0.17
[M-H+3O]	1.5E-4(3.0E-6)	2.7E-5(6.0E-6)	0.18
Au_2[M-H]	2.1E-4(4.3E-6)	2.8E-6(9.5E-7)	0.01
Au$[M-H]_2$	5.5E-5(1.1E-5)	5.8E-6(2.2E-6)	0.10
AuM	2.8E-4(1.9E-5)	1.5E-5(2.0E-6)	0.05
Characteristic Peaks			
CH_4N^+	4.1E-2(5.6E-4)	1.1E-3(3.6E-5)	0.03
NH_4^+	1.4E-2(2.4E-4)	9.2E-3(6.0E-5)	0.65

* Three samples were measured for each SAMs. Data shown are the average results with standard deviation (in brackets).

Table 5.4 Compositions of amino acids in $F(ab')_2$ and F_c fragments of anti-hCG from Protein Data Bank.

amino acids	$F(ab')_2$		F_c		ratio of $F(ab')_2/F_c$ composition
	# of groups	composition (%)	# of groups	composition (%)	
Alanine	48	5.43	18	4.39	1.24
Arginine	28	3.17	8	1.95	1.62
Asparagine	40	4.52	20	4.88	0.93
Aspartic acid	38	4.30	24	5.85	0.73
Cystein	18	2.04	8	1.95	1.04
Glutamine	34	3.85	22	5.37	0.72
Glutamic acid	40	4.52	26	6.34	0.71
Glycine	58	6.56	12	2.93	2.24
Histadine	10	1.13	14	3.42	0.33
Isoleucine	24	2.71	20	4.88	0.56
Leucine	58	6.56	18	4.39	1.49
Lysine	46	5.20	34	8.30	0.63
Methionine	18	2.04	8	1.95	1.04
Phenylalanine	26	2.94	24	5.58	0.50
Proline	48	5.43	34	8.29	0.65
Serine	132	14.93	30	7.32	2.04
Threonine	78	8.82	36	8.78	1.00
Tryptophan	18	2.04	8	1.95	1.04
Tyrosine	52	5.88	8	1.95	3.01
Valine	70	7.92	38	9.27	0.85

Table 5.5 Comparison of the relative prevalence of selected amino acids obtained from ToF-SIMS spectra with their composition ratio obtained from the protein structure.

amino acids more prevalent in $F(ab')_2$ from PCA of ToF-SIMS spectra	$F(ab')_2/F_c$ composition ratio from protein structure
Asparagine	0.93
Serine	2.04
Threonine	1.00
Tyrosine	3.01
Histadine	0.33
Tryptophan	1.04
amino acids more prevalent in F_c from PCA of ToF-SIMS spectra	**$F(ab')_2/F_c$ composition ratio from protein structure**
Lysine	0.63
Proline	0.65
Phenylalanine	0.50

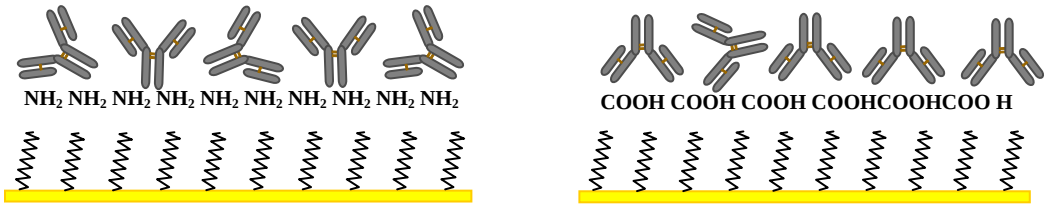

(a) (b)

Figure 5.1 Illustration of the orientations of anti-hCG immobilized onto (a) amino and (b) carboxyl terminated SAMs.

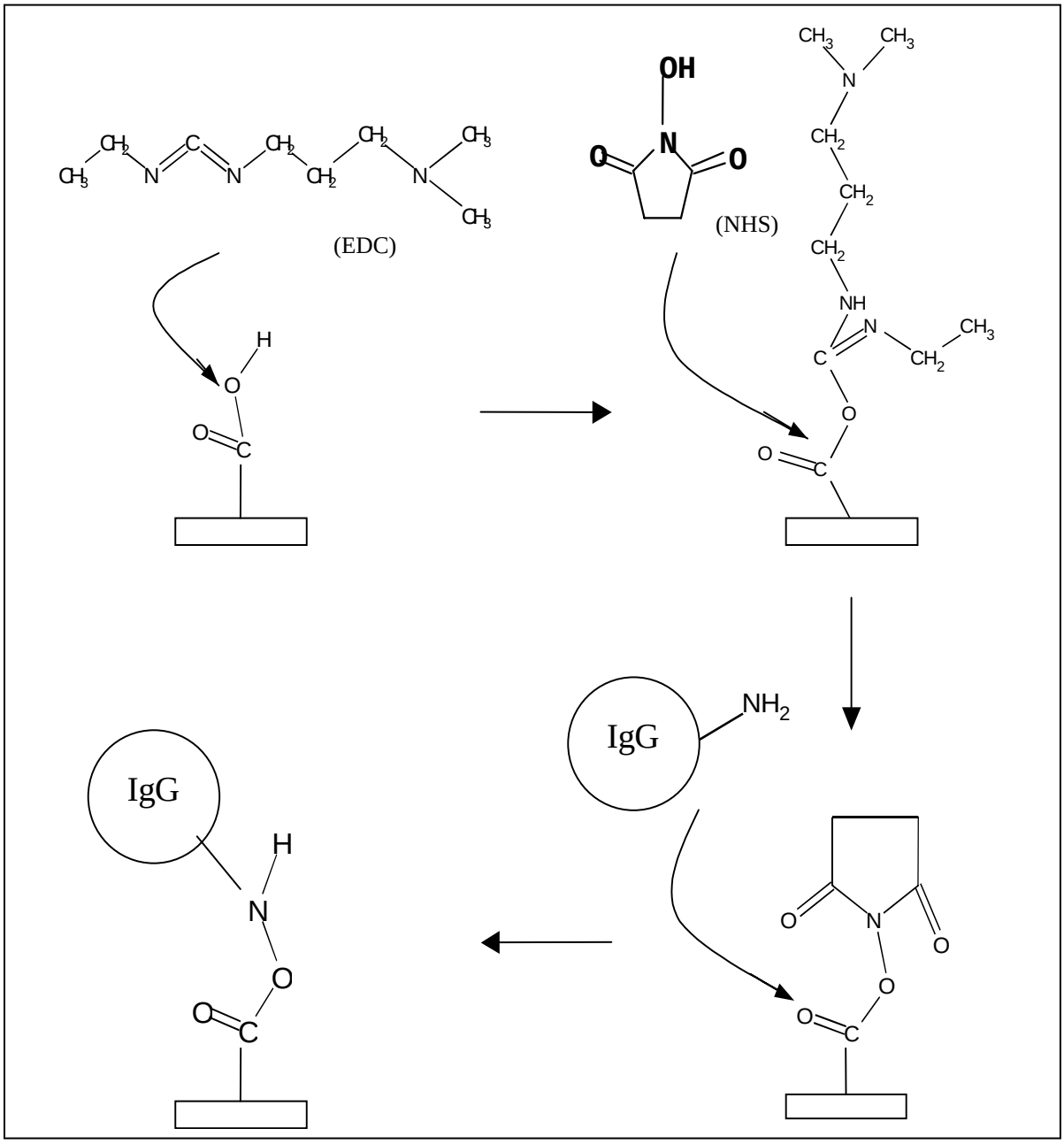

(a)

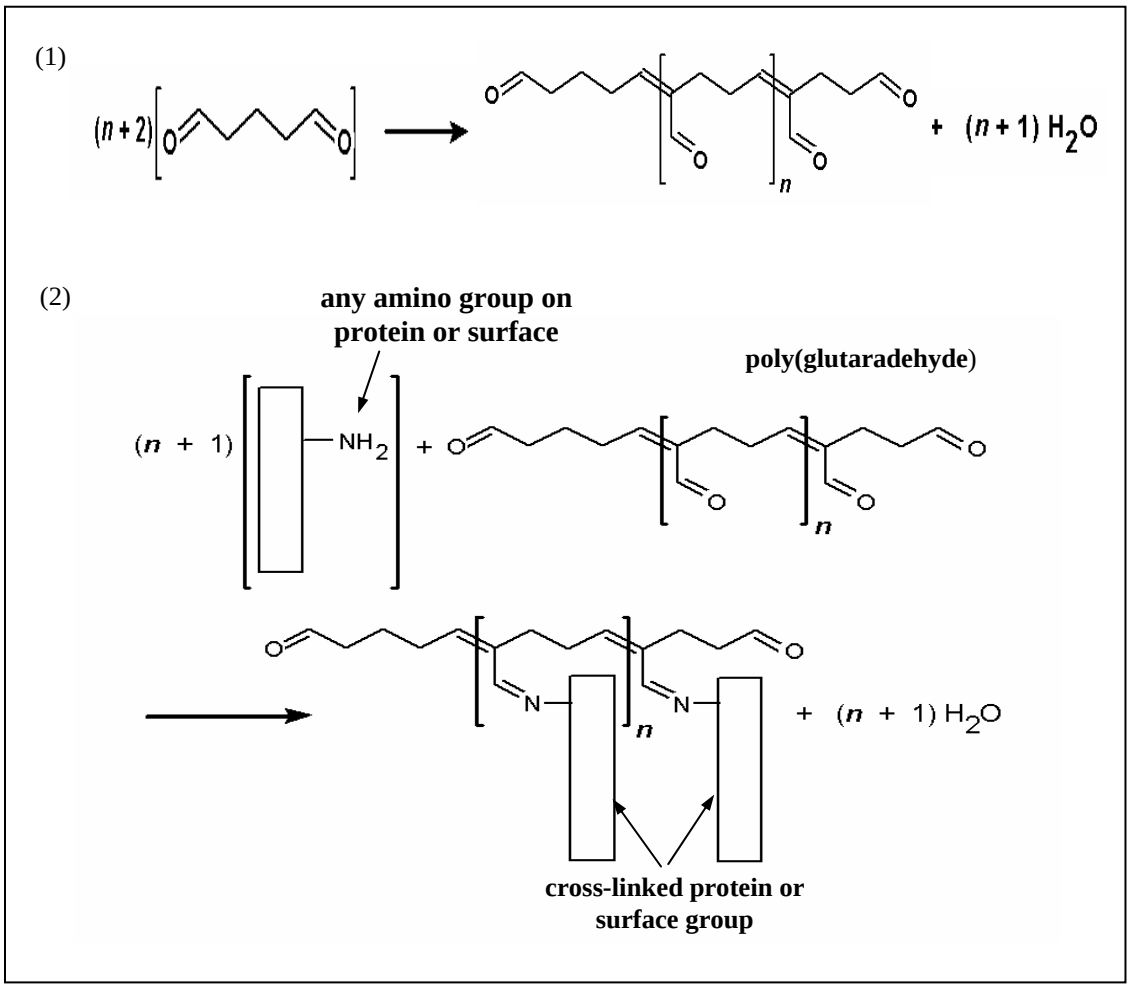

(b)

Figure 5.2 Schematic diagram showing the covalent attachment of IgG to the (a) carboxyl and (b) amino terminated SAMs via cross-linkers NHS/EDC and glutaraldehyde, respectively.

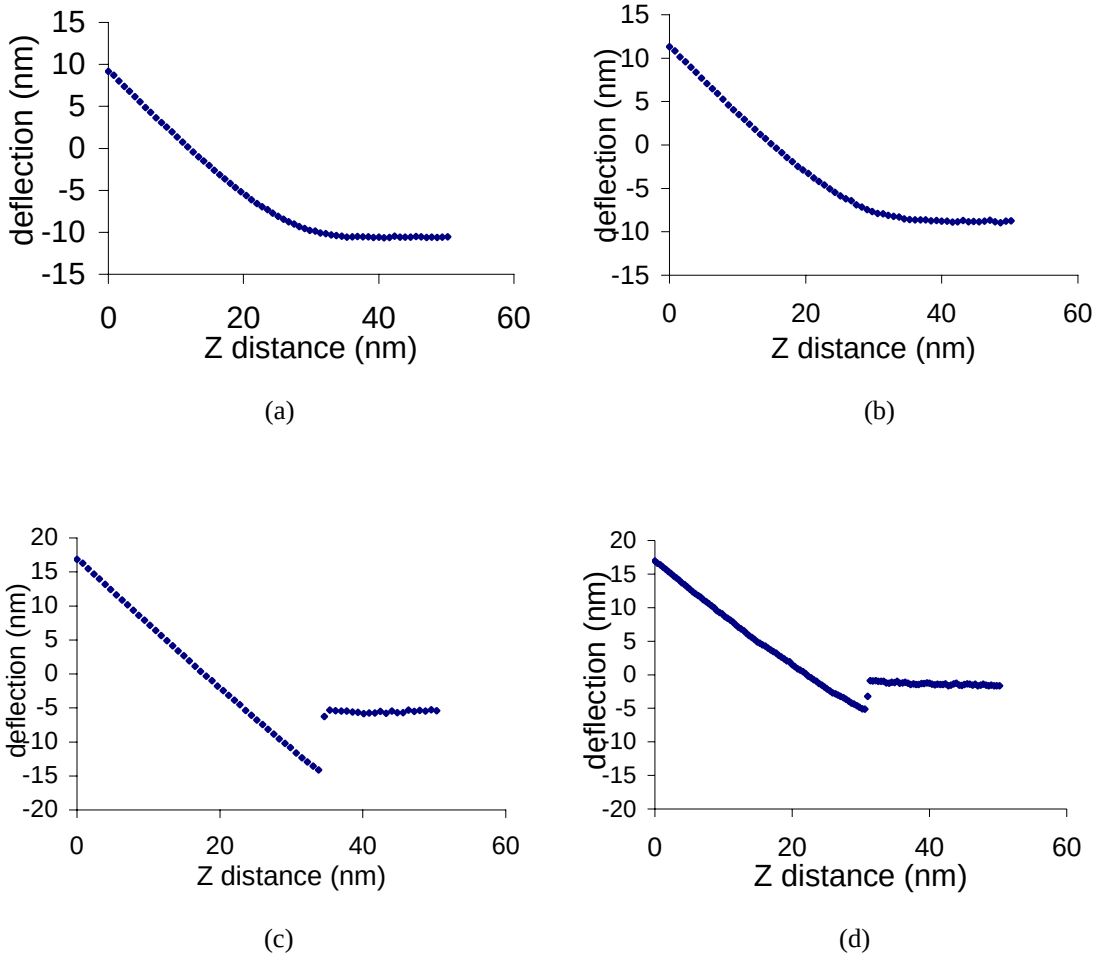

Figure 5.3 Force versus distance curves measured in 20 mM PBS (pH = 6.8) with a silicon nitride tip (k = 0.06 N/m) on (a) carboxyl terminated SAMs, (b) carboxyl terminated SAMs modified by NHS/EDC, (c) amino terminated SAMs, and (d) amino terminated SAMs modified by glutaradehyde. All curves show the approach of the tip to the sample.

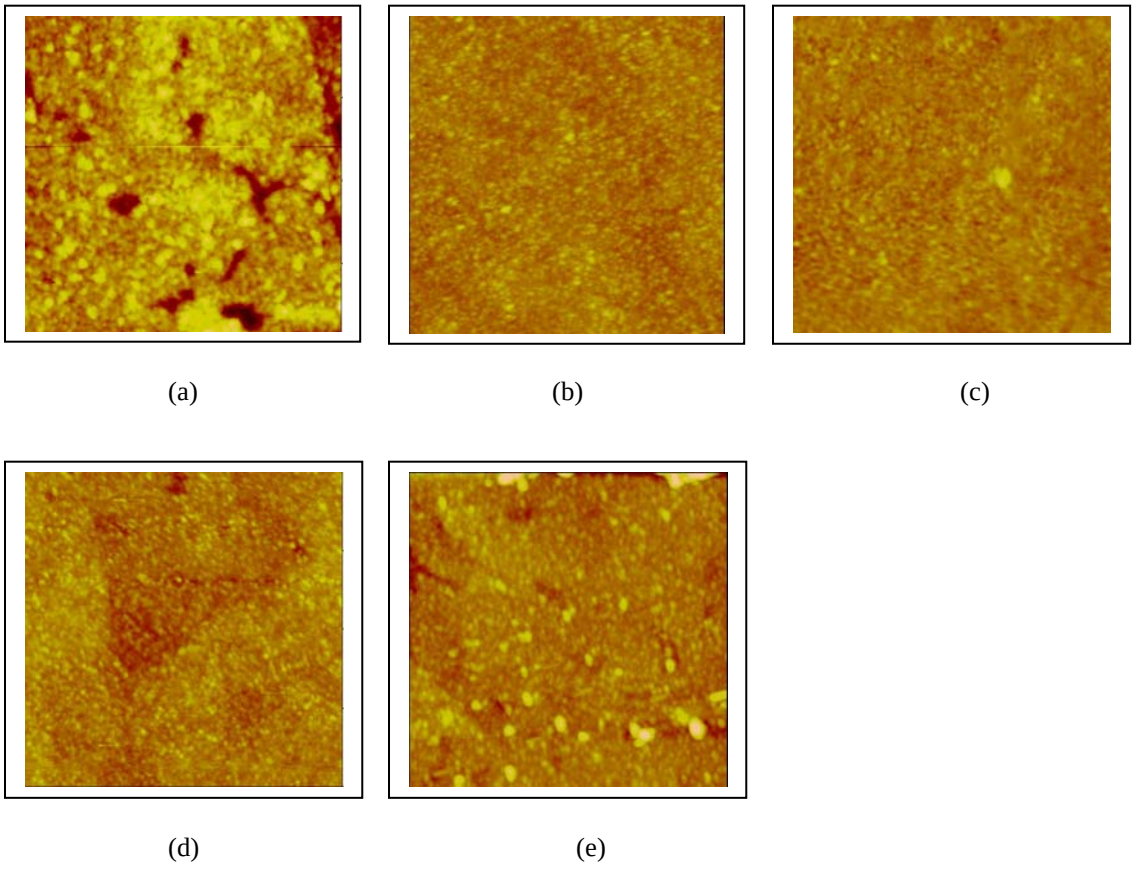

Figure 5.4 Tapping mode AFM images of (a) anti-hCG on carboxyl terminated SAMs, (b) anti-hCG on Au(111), (c) anti-hCG on amino terminated SAMs, (d) F(ab')$_2$ of anti-hCG on Au(111), and (e) F_c of anti-hCG on Au(111). Scanning areas are 1 µm × 1 µm for all images while height scale is 8nm.

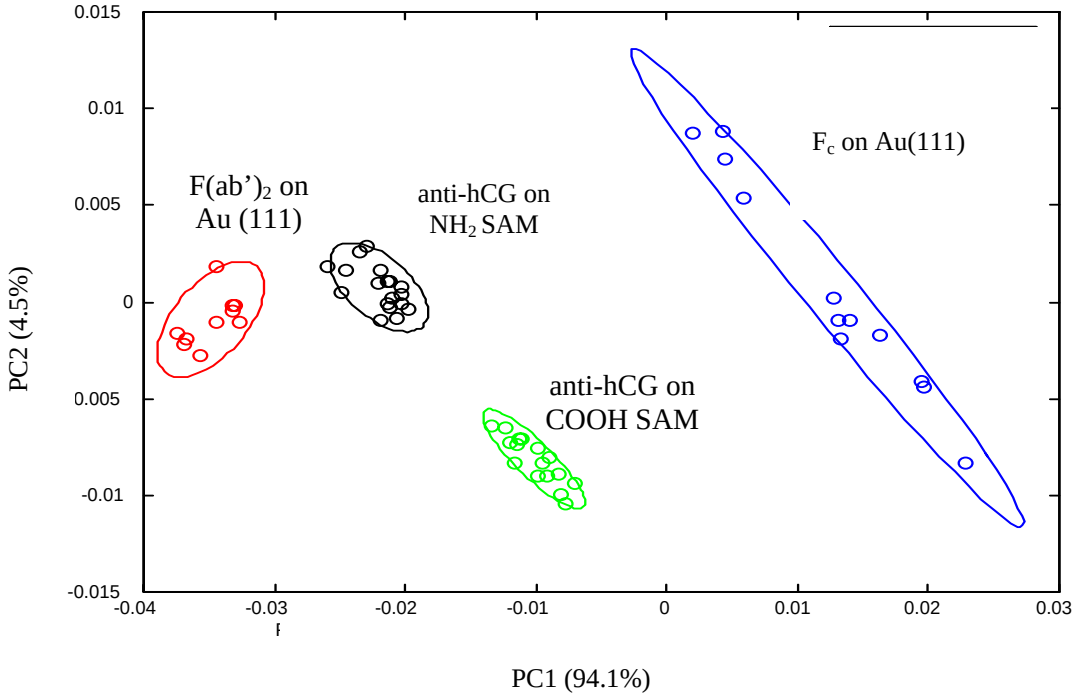

Figure 5.5 PCA scores plot of the positive ion ToF-SIMS spectra of anti-hCG immobilized onto carboxyl and amino terminated SAMs as well as its $F(ab')_2$ and F_c fragments adsorbed onto Au(111). The PCA model was developed using the first two PCs from PCA of the ToF-SIMS spectra of $F(ab')_2$ and F_c adsorbed onto Au(111).The ellipses drawn around each of the groups represent the 95% confidence limit for that group on PCs 1 and 2.

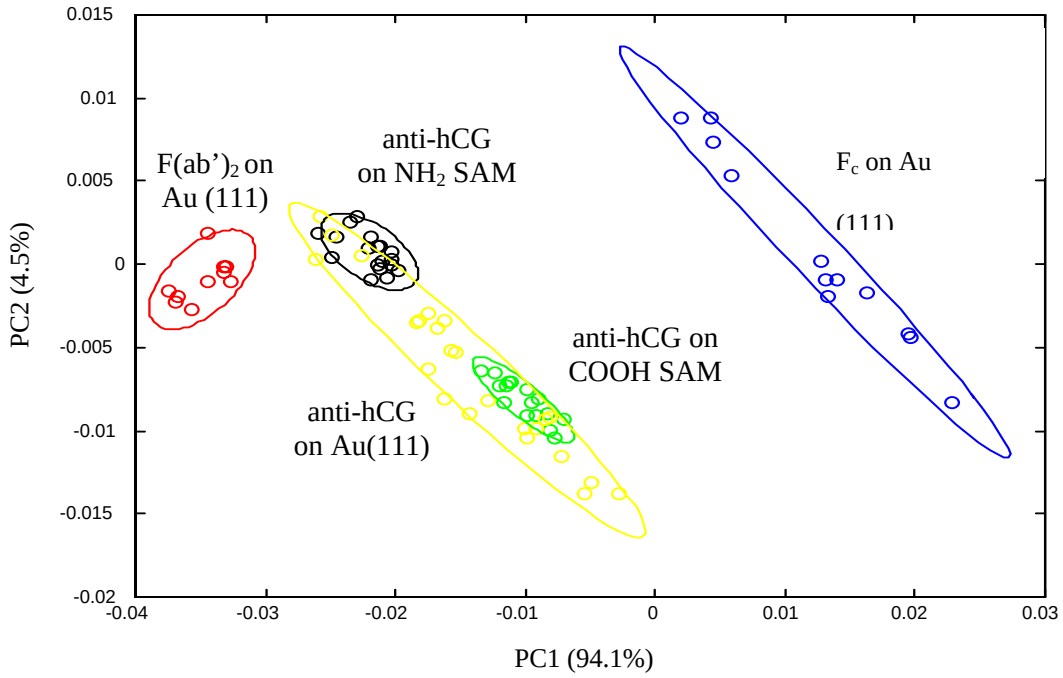

Figure 5.6 Similar to Figure 5.7, except that the PCA scores plot of the positive ion ToF-SIMS spectra of anti-hCG adsorbed onto Au(111) is added.

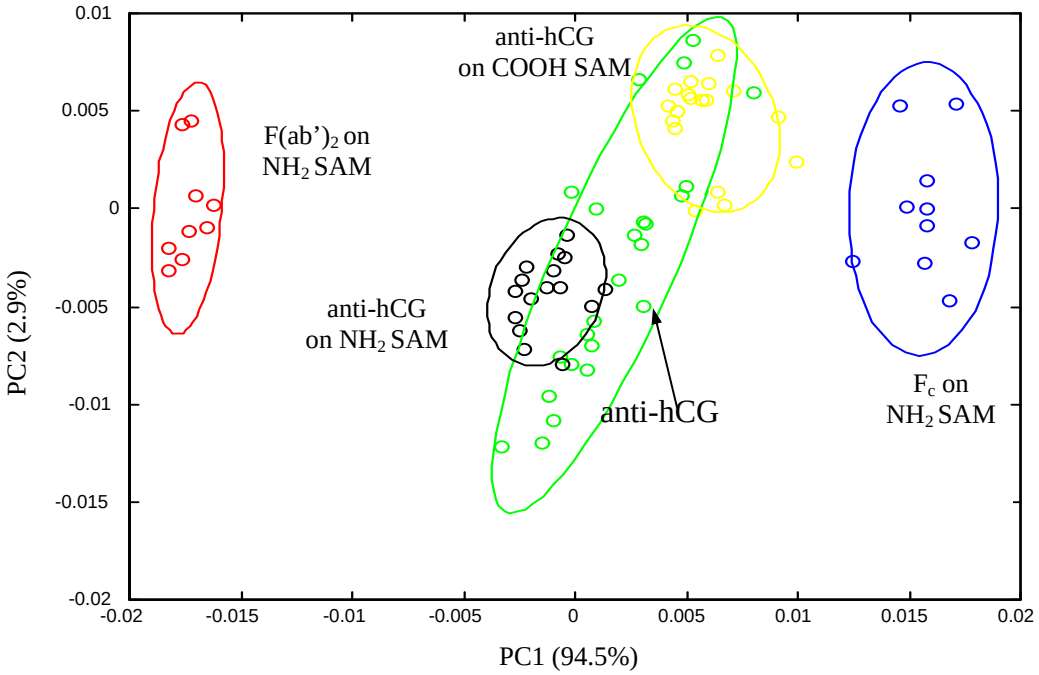

Figure 5.7 PCA scores plot of the positive ion ToF-SIMS spectra of anti-hCG adsorbed onto carboxyl and amino terminated SAMs and Au(111), as well as its F(ab')$_2$ and F$_c$ fragments adsorbed onto amino terminated SAMs. Unlike Figure 5.6, the PCA model here was developed using the first two PCs from PCA of the positive ion ToF-SIMS spectra of F(ab')$_2$ and F$_c$ adsorbed onto amino terminated SAMs. The ellipses drawn around each of the groups represent the 95% confidence limit for that group on PCs 1 and 2.

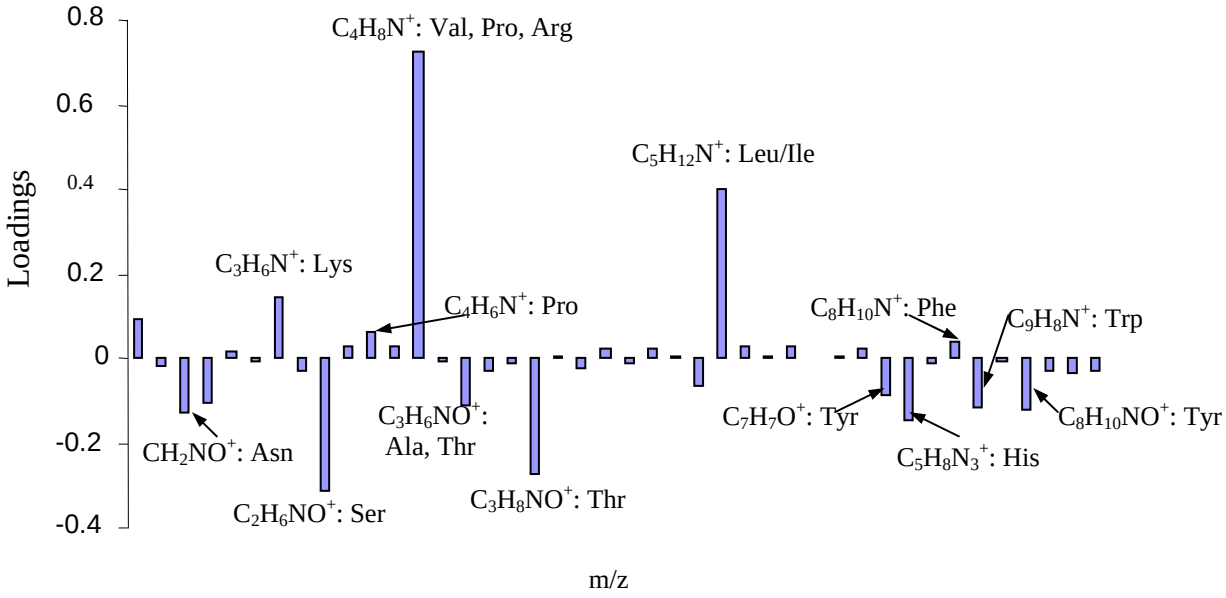

Figure 5.8 Loadings plot for the first PC in Figures 5.5 and 5.6. The loadings are ordered in increasing mass.

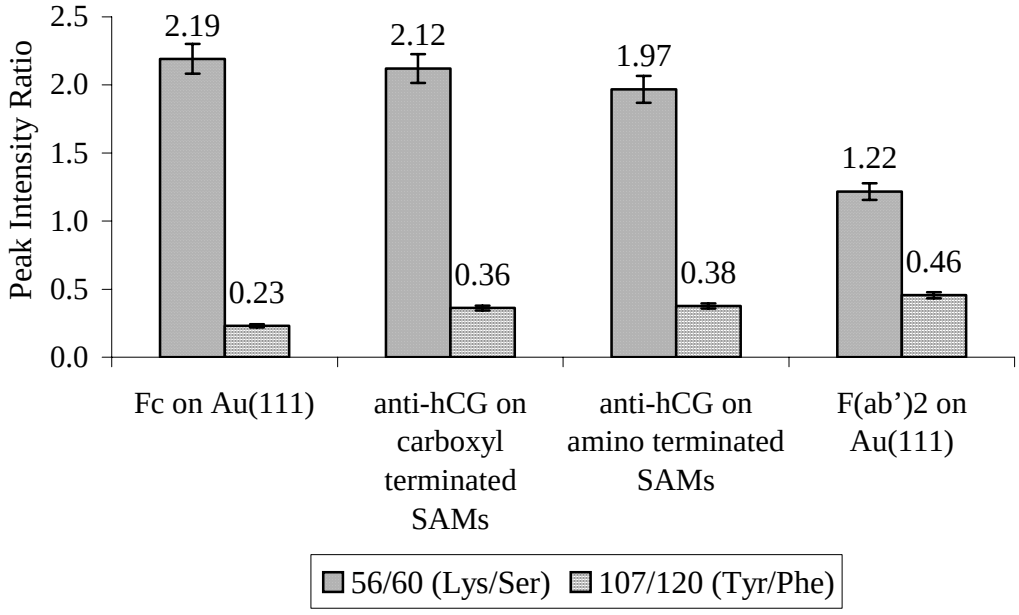

Figure 5.9 Peak intensity ratios for several protein layers from ToF-SIMS. The ratio of the 56 m/z (from Lys) to the 60 m/z (from Ser) peaks decreases while the ratio of the 107 m/z (from Tyr) to the 120 m/z (from Phe) peaks increases as more $F(ab')_2$ groups are positioned away from the substrate and exposed at the bulk surface. Data shown are the average results with standard deviation (error bar).

6. DNA-Directed Protein Immobilization on Mixed OEG and ssDNA SAMs

Sequence specificity and protein resistance: Control experiments were performed to test the sequence specificity and protein resistance of the DNA/OEG SAM surface. To test the specificity of hybridization to the surface bound ssDNA probes, the SPR response to both complement and non-complementary control oligonucleotide strands was measured. While the complement hybridized to the surface, there was no detectable binding of the non-complementary control sequence. Depending on the density of ssDNA probes, the complements hybridized with coverage in the range of $1 - 5 \times 10^{12}$ duplex/cm^2. This data is not shown because it is in agreement with previous results for DNA SAMs backfilled with mercaptohexanol, (MCH) [28].

High concentration solutions of BSA were used to check the protein resistance of the DNA SAM surfaces. **Figure 6.1** shows the SPR response of DNA SAMs with MCH and OEG backgrounds to a 1 mg/ml solution of BSA in Tris-EDTA NaCl, TE-NaCl. Whereas the DNA/MCH SAM rapidly and irreversibly adsorbs high amounts of BSA, the DNA/OEG SAM is protein resistant.

Finally, **Figure 6.2** shows the immobilization of complementary and non-complementary DNA-antibody conjugates onto a ssDNA (sequence A) probe surface. The antibody conjugates with the complimentary sequence, anti-hCG/c-A, bind to the surface due to sequence specific hybridization. The other antibody conjugates, anti-lysozyme/c-B, have a non-complementary sequence, and do not bind to the surface. In a similar manner, ssDNA/OEG SAMs prepared with the B sequence probes bind the anti-lysozyme/c-B conjugates, and resist the anti-hCG/c-A conjugate (not shown).

These control experiments clearly demonstrate that immobilization of the conjugates is controlled exclusively by sequence specific hybridization. The non-fouling OEG background prevents the protein segment of the conjugates, or any other protein for that matter, from non-specifically binding to the surface and the specificity of DNA hybridization ensures proper placement of the conjugates. As a result, it should be possible to apply a cocktail of different DNA-protein conjugates to a patterned ssDNA probe surface and let sequence specific hybridization direct the conjugates to the appropriate spots on the surface.

Surface optimization: DNA probe surface density was optimized to achieve maximal sensor performance. As described previously, the mixed ssDNA/OEG SAMs were prepared by co-adsorption from a mixed thiol solution containing ssDNA thiol and OEG thiol. The ssDNA thiol solution concentration was held constant, while the OEG thiol concentration was varied over a wide range of concentrations. Due to the competition between the two thiol components, the concentration of OEG thiol in the assembly solution determines the surface density of ssDNA probes, i.e. low OEG thiol concentrations result in

a SAM with a higher ssDNA probe density and high OEG thiol concentrations reduce the probe density. In order to determine the probe density that would immobilize the maximum amount of antibody conjugate, a series of ssDNA/OEG SAMs was prepared and conjugate hybridization was measured in situ by SPR. As shown in **Figure 6.3,** at high OEG concentrations, very little conjugate is immobilized because there is a low amount of ssDNA probes available on the surface. Once the OEG concentration drops below 25 μM, there is sufficient DNA on the surface to immobilize nearly a monolayer of antibody conjugates. As the OEG concentration is reduced further, the DNA probe density increases, until eventually, the ssDNA strands are packed so tight that the conjugates cannot penetrate the DNA SAM and hybridize. As a result, less DNA-antibody conjugate can be immobilized. To maximize conjugate coverage and sensor sensitivity all subsequent ssDNA/OEG SAMs were prepared with 100nM ssDNA thiol and 10 μM OEG thiol. Note that the optimal DNA probe density determined in this work depends on the size and shape of the protein immobilized. If a protein with a different footprint were used, the optimal DNA probe density would likely shift to reflect the change in protein packing.

Detection of hCG: Figure 6.4 shows the calibration curve for the detection of hCG. The lower limit of detection was 0.1 ng/ml and the response was linear for concentrations less than 100 ng/ml. For comparison, **Figure 6.4** also shows the detection of hCG using biotinylated anti-hCG which was immobilized via streptavidin on a mixed biotin and OEG SAM. For this system, the lower detection limit was 5 ng/ml, 50 fold higher.

The superior sensitivity of the DNA platform is likely due to the increased flexibility afforded by DNA. With DNA/OEG SAMs, it is possible to control the surface coverage of DNA probes in a continuous manner, for optimal antibody coverage. Immobilization of biontinylated antibodies on streptavidin, on the other hand, is less flexible due to the predefined distance between pockets in the streptavidin. The amount of streptavidin on the surface can be varied, but the distance between biotin binding spots cannot be changed. In addition, the 24 base pair long DNA used in this work acts like a molecular tether, and provides the immobilized antibody with greater mobility than a biotin/streptavidin linkage.

Surface regeneration: The DNA double helix can be dehybridized, or melted, by either chemical or thermal means. By dehybridizing the DNA duplex, the protein-DNA conjugates can be removed from the surface, thereby regenerating the ssDNA probe surface. This work used 0.05 M NaOH to dehybridize the DNA duplex and remove the conjugates from the surface.

Figure 6.5 shows a typical antigen detection and surface regeneration experiment. After equilibrating the surface with buffer, the conjugates are immobilized, antigen is detected, and the response is amplified with a secondary antibody. Once the detection is

complete, the NaOH solution is flowed for 5 minutes to dehybridize the DNA duplex and remove the conjugate and all associated proteins. The baseline returns to its original position, indicating that the DNA duplex has been dehybridized and the antibody conjugates and all associated protein material has been removed from the surface. The surface is completely regenerated. At this point, the antibody conjugate is immobilized a second time, and the hCG detection is repeated. **Table 6.1** compares the SPR response of the fresh DNA surface with the regenerated surface for each step in the hCG detection. Note that the regenerated DNA/OEG surface immobilized the same amount of antibody conjugate as the fresh chip, and that the responses to hCG and the secondary antibody are also comparable.

Surface regeneration is a desirable feature for any sensor that is operated in a remote or potentially dangerous environment. Instead of requiring a person to manually change the sensor chip, it can be regenerated with NaOH, and used again for a new detection. In the experiment described above, we used a sensor chip for two consecutive detections of the same analyte, but a regenerated chip could also be used for detection of an entirely different analyte.

Table 6.1 Comparison of SPR response for detection of hCG on fresh and regenerated surface.

	SPR Response (nm)		
Chip surface	**anti-hCG conjugate**	**hCG (5 mg/ml)**	**polyclonal anti-hCG**
Fresh	16.6	3.6	34.2
Regenerated	16.8	3.2	28.3
Efficiency	101%	89%	83%

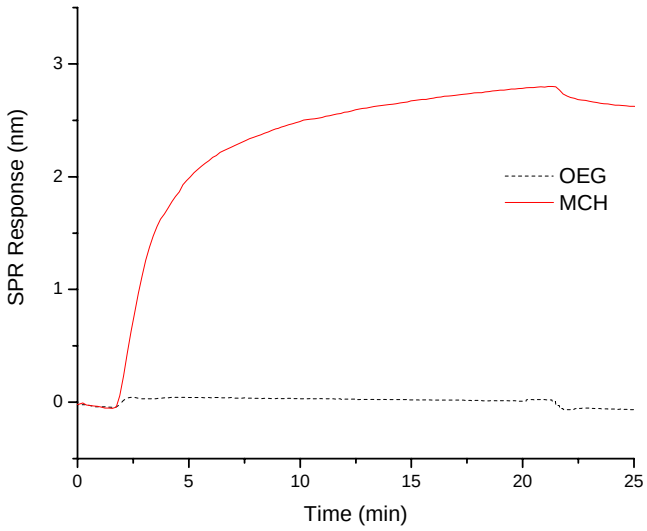

Figure 6.1 Testing protein resistance. BSA (1 mg/ml) was flowed over ssDNA SAMs prepared with MCH and OEG diluent thiols. The surface prepared with OEG is completely protein resistant.

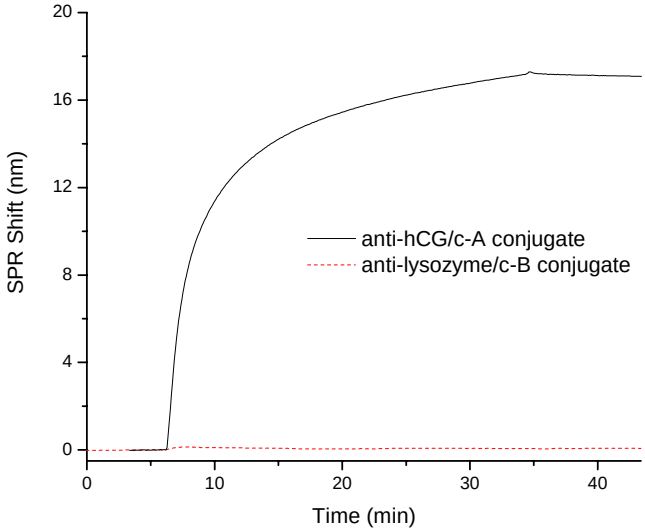

Figure 6.2 Control experiment to test for conjugate immobilization specificity. Both anti-hCG/c-A and anti-lysoyzme/c-B conjugates were flowed over a sequence A ssDNA/OEG SAM, but only the conjugate with the complimentary sequence bound to the surface

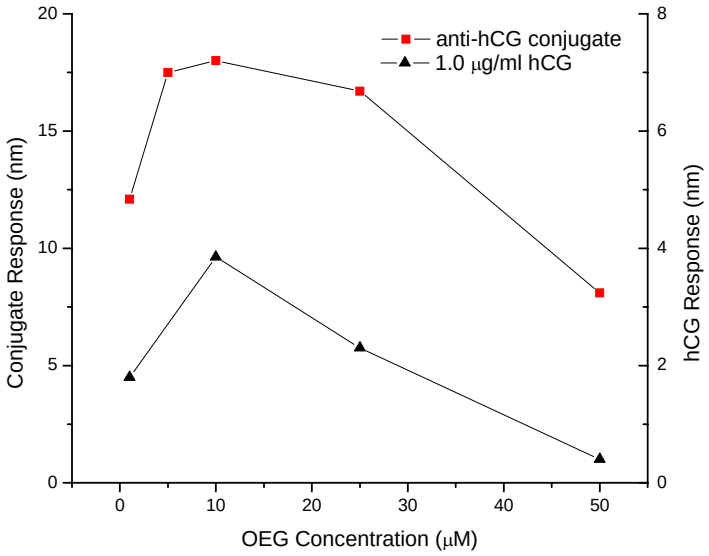

Figure 6.3 Optimization of surface composition for maximum conjugate binding. Mixed ssDNA/OEG SAMs were prepared with various amounts of OEG thiol, and the amount of conjugate and antigen that bound to each surface was measured. A ssDNA probe surface with 100 nM ssDNA thiol and 10 μM OEG thiol was found to bind the most conjugate.

(a) (b)

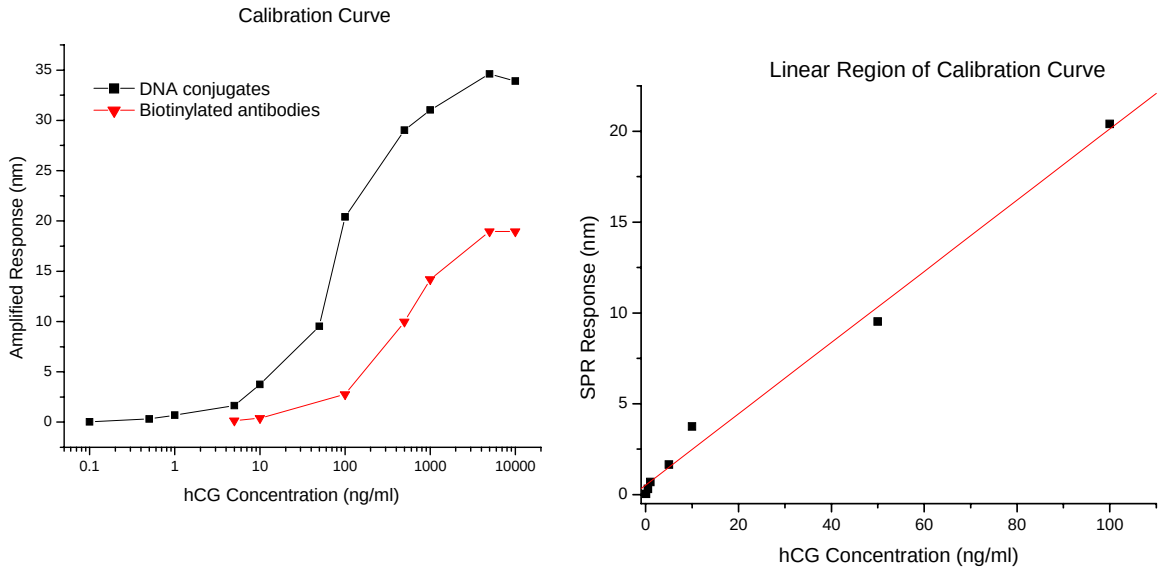

Figure 6.4 (a) Calibration curve for the detection of hCG. The lowest detection limit was 0.1 ng/ml hCG. (b) Linear region of detection curve.

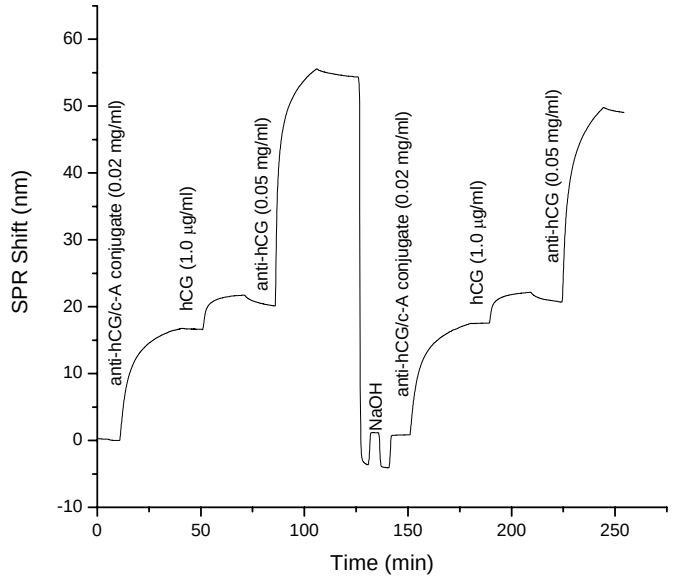

Figure 6.5 Recycling of DNA probe surface. A typical hCG detection experiment was run and 50 mM NaOH was used to dehybridize the DNA duplex. After dehybdridization, all conjugate and protein is removed from the surface and a second detection was performed.

7. DNA-Directed Protein Immobilization on SAMs via a Streptavidin Bridge

Non-Fouling Surface. The OEG/BAT mixed SAM provides a non-fouling background for the binding of streptavidin onto the surface [29,30]. This is due to the OEG portion of the BAT behind the biotin head group and the rest of the OEG background. Once the streptavidin and biotinylated oligonucleotide are on the surface, the non-fouling properties of this surface may change considerably. A non-fouling surface is a necessity for sensor chips. If the surface used for sensing fouls, or non-specifically adsorbs large amounts of protein, the detection response cannot be validated. This will result in false detections.

The sensor surface used in this work maintains its non-fouling characteristics following the immobilization of streptavidin and the biotinylated oligonucleotide. **Figure 7.1** shows the specificity of the DNA surface to the complementary antibody-DNA conjugates. An antibody conjugated to a non-complimentary oligonucleotide is flowed across the surface. A minimal (~ 0.1 nm) binding response is observed. This binding is less than 1% of the binding seen when an antibody conjugated to a complimentary oligonucleotide is passed across the surface. **Figure 7.2** shows the non-specific adsorption of the mouse monoclonal anti-hCG antibody used in the conjugation procedure. Again, minimal non-specific binding (< 0.1 nm) is seen. These data show the sensor surface does not non-specifically bind non-complimentary conjugates and the binding of the complimentary conjugates is due to DNA hybridization and not non-specific adsorption of the antibodies present in the conjugates.

Antibody-DNA Conjugate Surface Coverage Optimization. Antibody-DNA conjugate surface coverage was optimized based on oligonucleotide surface density. A comparison of conjugate responses from solutions of PBS and Tris-EDTA (TE) (10 mM Tris, 5 mM EDTA, pH 7.4) was made. The TE buffer showed a slight increase (~ 10%) in conjugate binding compared to the PBS buffer (data not shown).

Surface coverage can be approximated using the following equation:

$$\delta\lambda_{res} = S_S \cdot \Gamma \cdot \frac{\partial n}{\partial c}$$

where $\delta\lambda_{res}$ is the observed wavelength shift, S_S is the surface refractive index sensitivity, Γ is the surface coverage, and $\frac{\partial n}{\partial c}$ is the inverse slope coefficient relating refractive index to concentration. The sensitivity of the SPR sensor is dependent on the wavelength of the resonant dip. In this work, a resonant dip corresponding to a value of S_S of ~ 42 was used. Values for $\frac{\partial n}{\partial c}$ for proteins are typically ~ 0.15 – 0.2 cm^3/g. In these calculations, a value of 0.17 was used for proteins, while a value of ~ 0.14 cm^3/g for DNA molecules was used.

Theoretical calculations based on the footprint size of an IgG antibody show a monolayer of antibody corresponds to a coverage of ~295 ng/cm^2 (1.18×10^{12} molecules/cm^2). Assuming a 1:1 correspondence between surface-bound bDNA and conjugate, a theoretical minimum coverage of 1.18×10^{12} molecules/cm^2 of bDNA is necessary to immobilize a monolayer of antibody. Above this bDNA coverage a monolayer of immobilized antibody should be observed. These theoretical values are calculated under the assumption of having perfect packing densities of non-interacting molecules. Due to irregularly shaped molecules with surface charges, actual values will deviate from the above theoretical calculations.

Experimentally, a 100 nM solution of biotinylated DNA in TE with 1 mg/mL BSA was flowed across a surface with immobilized streptavidin for varying times to control the surface coverage of the DNA. Conjugate was then bound to the immobilized DNA. A maximum conjugate binding was seen at a DNA coverage of ~2.25 x 10^{12} molecules/cm^2, shown in **Figure 7.3.** This DNA coverage corresponded to an observed plateau in the SPR response to the DNA. The observed shift away from the minimum necessary DNA coverage is most likely due to electrostatic hindrances and the discrete spacing of binding sites on the streptavidin. The buffer used during immobilization has 100 mM NaCl, which is not sufficient to screen the electrostatic repulsion observed during DNA hybridization. Higher salt concentrations could be used to decrease this effect, but these higher concentrations also denature the antibody, decreasing its activity. Biotinylated DNA strands can only bind to the binding pockets in streptavidin, and consequently, cannot position itself at an optimal distance from other strands immobilized to the streptavidin.

hCG Detection Using Optimized Platform. A detection curve was generated from SPR responses to hCG flowed across the surface. A secondary antibody can be used to amplify the detection signal and further verify detection of analyte. This secondary antibody binds to epitopes on the analyte different from those recognized by the monoclonal antibody-DNA conjugate. This specific binding produces a much larger SPR response if antigen is present, and removes speculation of a false positive, if the secondary antibody does not non-specifically bind to the sensor surface.

This detection data was compared to data obtained from using a biotinylated antibody platform. The attachment of the biotin to the antibodies in this previous work was done using a similar attachment scheme via the amine groups on the antibody surface. **Figure 7.4a** shows a comparison between the detection levels of the two platforms. The antibody-DNA conjugate platform improves the lower detection limit by one order of magnitude (0.5 ng/mL vs. 5 ng/mL) as seen in **Figure 7.4b**. This increase in lower limit sensitivity could be attributed to an increased flexibility granted to the immobilized antibodies by the longer length of the DNA tether compared to a biotin linkage. A detection saturation limit is seen at

roughly the same concentration (5 μg/mL). The dynamic detection range for the antibody-DNA conjugates covers a larger range of analyte concentrations. At low limits, the amplification detection responds linearly with respect to analyte concentration.

A low limit detection, as seen in **Figure 7.5a**, was observed for 0.5 ng/mL. Detection at a concentration of 0.1 ng/mL, **Figure 7.5b**, was tested, but could not be distinguished from signal drift. This demonstrates the usefulness, and oftentimes the necessity, of having a reference channel when detecting low concentrations of analyte. The ability to distinguish between an actual detection and a false positive is enhanced by using a reference channel.

Multiple Proteins in Solution. A mixture of anti-hCG and anti-lysozyme conjugates was tested to determine if any cross hybridization, and subsequent false detection, would occur within a flow channel. The same bDNA sequence A is immobilized in each flow channel. **Figure 7.6** shows two channels on a dual-channel chip comparing the response from a pure conjugate solution detecting a pure antigen to that of a mixture of conjugates detecting a mixture of antigens. Anti-lysozyme conjugated to ssDNA sequence c-B is flowed across both channels, showing a negligible response in both channels. Following a wash with buffer, complimentary anti-hCG conjugate is flowed across the surface. In one channel, pure anti-hCG conjugate is flowed. The other channel contains a mixture of complimentary anti-hCG conjugate and non-complimentary anti-lysozyme conjugate. In the mixture solution, each component is at the same concentration as the pure conjugate. The responses for conjugate binding for the two channels are within 1% of each other. This indicates the same amount of antibody is binding to the surface regardless of the presence of other conjugates in the solution. The channel with the mixture of conjugate shows slightly slower kinetics. This is most likely due to a diffusive hindrance caused by the increased amount of non-interacting protein in solution. Analyte detections behave in a similar manner to the conjugate detections. Final responses are within 3% of each other, which is within experimental variation for single protein solutions. The kinetics of the mixture are, as with the conjugates, slower.

.

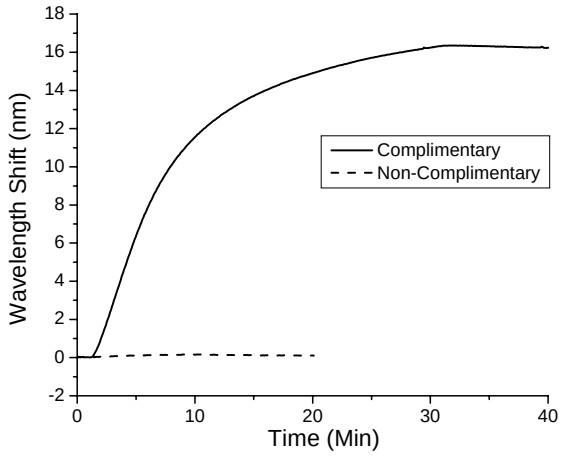

Figure 7.1 The response from a non-complimentary antibody-DNA conjugate is less than 1% of the complimentary conjugate response. The lack of response from the non-complementary conjugate shows the specificity of the DNA immobilization platform.

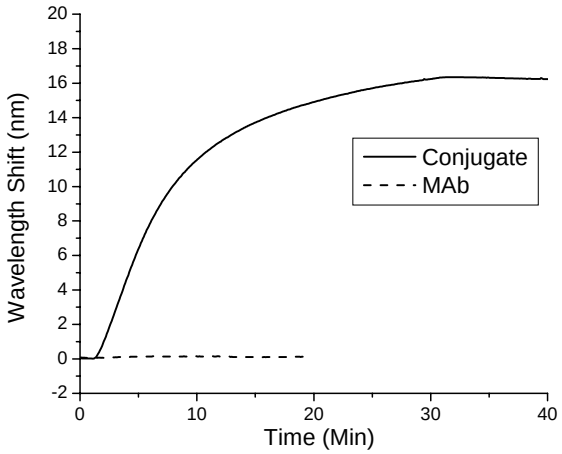

Figure 7.2 The response from the monoclonal antibody used in forming the anti-hCG conjugates is less than 1% of the conjugate response. The lack of response from the monoclonal antibody shows the binding that is occurring is due to DNA hybridization.

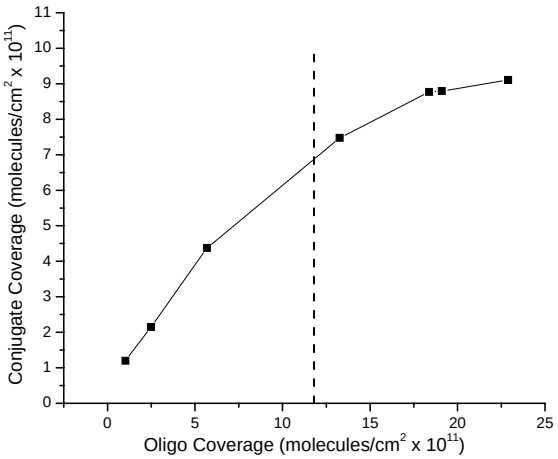

Figure 7.3 Conjugate surface coverage as a function of DNA coverage. Dashed line indicates theoretical oligo coverage necessary for a monolayer of conjugate (1.18 x 10^{12} molecules/cm^2). The coverage corresponding to the maximum conjugate binding is higher than the theoretical value, indicating the DNA molecules on the surface are not optimally (ideally?) spaced for conjugate binding

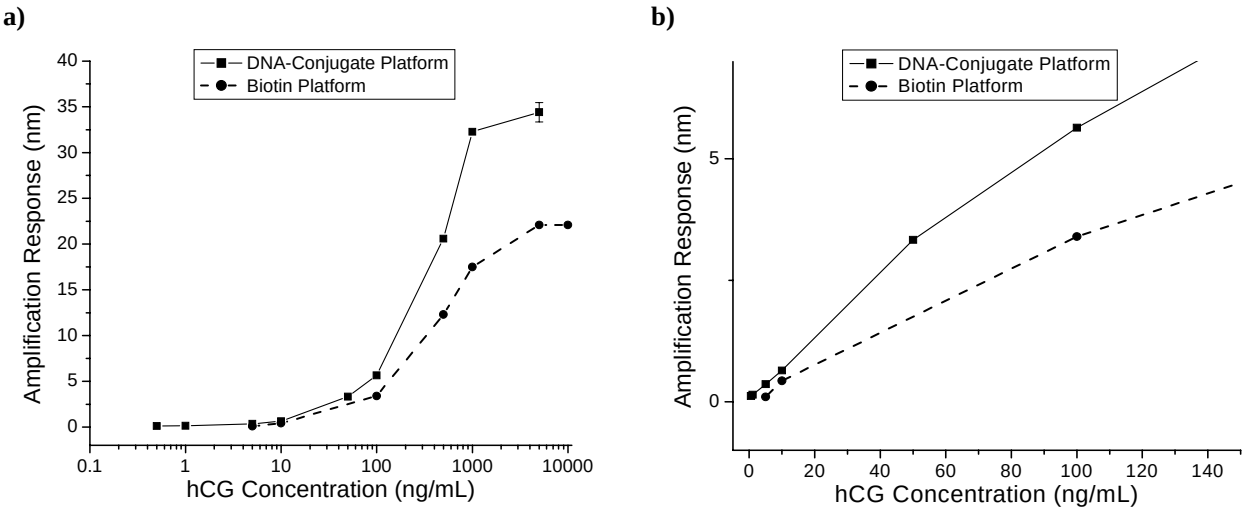

Figure 7.4 hCG detection curve comparison of antibody-DNA conjugate platform and biotinylated antibody platform a) over the entire range of detection from lowest detection limit to saturation and b) showing a close-up of the linearity of the low detection region.

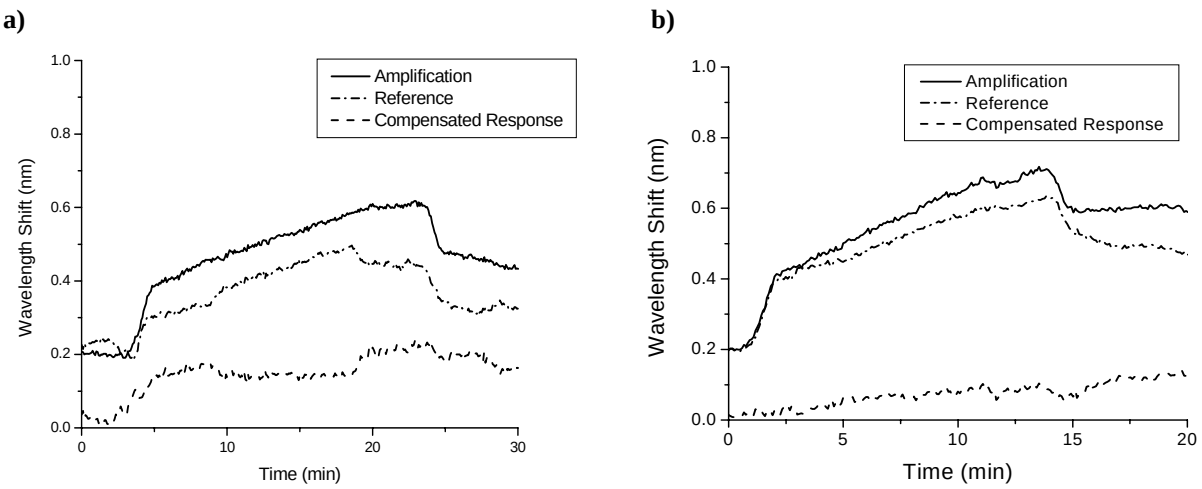

Figure 7.5 Compensated SPR response showing a) a detection of 0.5 ng/mL and b) no clear detection of 0.1 ng/mL. A reference channel is used to remove the bulk refractive index changes from the detection response.

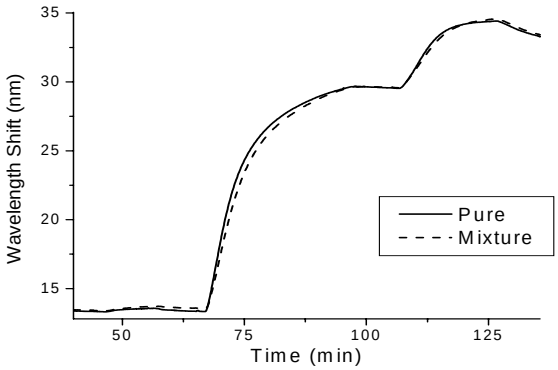

Figure 7.6 SPR responses from a mixture of proteins in solution compared to a solution containing only one protein. Similar responses show the specificity in conjugate binding and detection.

Conclusions

In this work, we proposed a charge-driven protein orientation principle, which is of general significance and is applicable to many systems. Our molecular simulation and experimental results have confirmed the charge-driven protein orientation. Recently, we have applied this principle to control of the orientations of several cell-binding proteins with great success. Our recommendation for future work is to study protein conformation in detail while further improving the control of protein orientation.

In this work, we proposed a DNA-directed protein immobilization technique to create a protein array from a DNA array. The integration of this protein immobilization technique with biosensors (all types) will make biosensors very powerful, including their robustness for multiple channels, stability for long-term chip storage, convenient chip regeneration, and one universal chip for all applications, in addition to high sensitivity and specificity. Our recommendation for the future work is to demonstrate this array capacity on silicon chips.

In this work, we initiated a study on control of nonspecific adsorption, which is also another important issue in biosensors. This work was later supported by NSF for the studies of the molecular-level non-fouling mechanism. Recently, we are designing new-generation non-fouling materials for marine coatings supported by Office of Naval Research (ONR).

The combination of three unique capacities developed in this work relating to surface chemistries for biosensors has put us into a unique position in the area of sensing and detection. We are developing a biosensor system for the U.S. FDA and applying our sensor technology to food safety and security monitoring. In addition, we are working with several collaborators to apply our sensor technology to biomedical diagnostics. This technology has also transferred to a company (ANP) and a DOE collaborator for the detection and identification of biological warfare agents. Furthermore, our computational capacities supported by this program have further evolved into a stage that we are able to rationally design non-fouling biomaterials.

References

[1] Buijs, J.; White, D.D.; and Norde, W. *Colloids and Surface B* **1997**, 8, 239.

[2] Edmiston, P. L.; Wood, L., L.; Lee, J. E.; and Saavedra, S. S., *J. Phys. Chem.* **1996**, *100*, 775.

[3] Chi, Q.J.; Zhang, J.D.; Andersen, J.E.T.; and Ulstrup, J., *J. Phys. Chem., B* **2001**, 105, 4669.

[4] Ahluwalia, A.; Rossi, D.D.; Ristori; C.; Schirone, A.; and Serra G., *Biosensors& bioelectronics*, **1991,** 7, 207.

[5] Ravichandran, S., Madura J. D. and Talbot, J., *J., Phys. Chem. B,* **105**, 3610 (2001).

[6] Bushnell, G. W.; Louie, G. V.; and Brayer, G. D., *J. Mol. Biol.*, **1990**, *214*, 585.

[7] Chen, X.X.; Ferrigno, R.; Yang, J.; and Whitesides, G.A., *Langmuir*, **2002**, 18, 7009.

[8] Beglov, D. and Roux, B., *J. Chem. Phys.*, **1994**, *100*, 9050.

[9].Noinville,V., Vidal-Madjar, C., and. Sebille B., *J Phys. Chem*., **1995**, 99, 1516.

[10] Roush, D. J.; Gill, D. S.; and Willson, R. C., *Biophys., J.,* **1994**, *66*, 1290.

[11] Lu, D. R. and Park, K., *J. Biomater. Sci. Polym. Ed,*. **1990**, *4*, 243.

[12] Juffer, A. H.; Argos, P. and DeVlieg, J, *J. Comput. Chem.*, **1996**, *17*, 1783.

[13] Ball, V. and Ramsden, J. J., *J. Phys. Chem. B,* **1997**, *101*, 5465.

[14] Ben-Tal, N.; Honig, B.; Peitzsch, R. M.; Denisov, G; and McLaughlin, *Biophys. J.*, **1996**, *71*, 561.

[15] Roth, C. M., and Lenhoff, A.M., *Langmuir*, **1993**, 9, 962.

[16] San Paulo, A.; and Garcia, R., *Biophys. J.*, **2000**, *78*, 1599.

[17] Du, Y. Z.;and Saavedra, S. S., *Langmuir*, **2003**, 19, 6443.

[18] Fedurco, M., *Coordin. Chem. Rev*., **2000**, *209*, 263.

[19] Burkett, S. L.; and Read, M. J., *Langmuir*, **2001**, *17*, 5059.

[20] Stocker, U.; Spiegel, K.; and van Gunsteren, W. F., *J. Biomol, NMR*, **2000**, *18*, 1.

[21] Silin, V.; Weetall, H.; and Vanderah, D.J.; *J Colloid Interf Sci*, **1997**, 185, 94.

[22] Nordgren, C. E.; Tobias, D. J.; Klein, M. L.; and Blasie, J. K., *Biophys. J.*, **2002**, *83*, 2906.

[23] Tobias, D. J.; Mar, W.; Blasie, J. K., and Klein, M. L., *Biophys. J.*, **1996**, *71*, 2933.

[24].Chen, S., Liu L, Zhou J,and Jiang S., *Langmuir*, **2003**, 19, 2859.

[25] Butt, H.J., *Biophysical Society*, **1992**, 63, 578.

[26] www.pdb.org.

[27] Lhoest, J.B.; Wagner, M.S.; Tidwell, C.D.; and Castner, D.G., *Journal of Biomedical Materials Research.* **2001,** 57, 432.

[28] Herne, T.M. and Tarlov M.J., *Journal of the American Chemical Society*, **1997**, 119, 8916.

[29] Nelson, K. E.; Gamble, L.; Jung, L. S.; Boeckl, M. S.; Naeemi, E.; Golledge, S. L.; Sasaki, T.; Castner, D. G.; Campbell, C. T.; and Stayton, P. S., *Langmuir* **2001**, *17*, 2807.

[30] Jung, L. S.; Nelson, K. E.; Stayton, P. S.; Campbell, C. T., *Langmuir*, **2000**, *16*, 9421.

[31] Ramsden, J. J.; Roush, D. J.; Gill, D. S.; Kurrat, R.; and Willson, R. C., *J. Am. Chem. Soc.*, **1995**, *117*, 8511.

Publications under this DARPA Support

1. J. Zhou, H.K. Tsao, Y.J. Sheng, and S. Jiang, Adsorption and Orientation of Model Antibodies on Charged Surfaces: A Monte Carlo Simulation Study, *Journal of Chemical Physics*, **121**, 1050 (2004); (b) Y.J. Sheng, H.K. Tsao, J. Zhou, and S. Jiang, Orientation of a Y-Shaped Biomolecule Adsorbed on a Charged Surface, *Physical Review E*, 66 011911 (2002).
2. J. Zhou, S. Chen, and S. Jiang, Orientation of Adsorbed Antibodies on Charged Surfaces by Computer Simulation Based on a United-Residue Model, *Langmuir,* **19** , 2859 (2003).
3. J. Zhou, J. Zheng, S. Jiang, Molecular Simulation Studies of Orientation and Conformation of Cytochrome c Adsorbed on Self-Assembled Monolayers, *Journal of Physical Chemistry B*, **108**, 17418 (2004).
4. S. Chen, L. Liu, J. Zhou, S. Jiang, Controlling Antibody Orientation on Charged Self-Assembled Monolayers, *Langmuir*, **19** , 2859 (2003).
5. H. Wang, D. Castner, B.D. Ratner, and S. Jiang, Probing the Orientation of Surface-Immobilized IgG by ToF-SIMS, *Langmuir*, **20**,1877 (2004).
6. C. Boozer, J. Ladd, S. Chen, Q. Yu, J. Homola, S. Jiang, DNA Directed Protein Immobilization on Mixed ssDNA/Oligo(ethylene glycol) Self-Assembled Monolayers for Sensitive Biosensors, *Analytical Chemistry*, **76**, 6967 (2004).
7. J. Ladd, C.L. Boozer, Q. Yu, S. Chen, J. Homola, S. Jiang, DNA-Directed Protein Immobilization on Mixed Self-Assembled Monolayers via a Streptavidin Bridge, *Langmuir*, **20**, 8090 (2004).
8. J. Zhou, L. Zhang, Y. Leng, H.K. Tsao, Y.J. Sheng, and S. Jiang, Unbinding of the Streptavidin-Biotin Complex by AFM: A Hybrid Simulation Study. Submitted to *Biophysics Journal* (2005).

List(s) of Symbols, Abbreviations, and Acronyms

AFM - Atomic force microscopy
BSA - Bovine serum albumin
CHARMM - (Chemistry at HARvard Molecular Mechanics) is a program for macromolecular simulations, including energy minimization, molecular dynamics and Monte Carlo simulations. http://yuri.harvard.edu/
EDTA - Ethylene Diamine Tetraacetic Acid
hCG - Human Choriogonadotropin
IgG - Immunoglobulin G
IgY - Immunoglobulin Y
SPR - Surface plasmon resonance
IEP - Isoelectric point
LJ - Lennard-Jones
MD - Molecular dynamics
MC - Monte Carlo
OEG - Oligo(ethylene glycol)
PBS - Phosphate Buffered Saline
PCA - Principal Components Analysis
RATTLE - Andersen, H. C. Rattle: A 'Velocity' Version of the Shake Algorithm for Molecular Dynamics Calculations. J. Chem. Phys., 52, pp 24-34, 1983.
SAM - Self-assembled monolayer
TIP3P - W.L. Jorgensen; J.Chandrasekhar; J.D. Madura; R.W. Impey; M.L. Klein; "Comparison of simple potential functions for simulating liquid water", J. Chem. Phys. 79 926-935 (1983).
TOF-SIMS - Time-of-flight secondary ion mass spectrometry
VDW - Van Der Waals
XPS - X-ray photoelectron spectroscopy